International Journal of Applied Earth Observations and Geoinformation 112 (2022) 102957

Contents lists available at ScienceDirect

International Journal of Applied Earth Observation and Geoinformation

journal homepage: www.elsevier.com/locate/jag

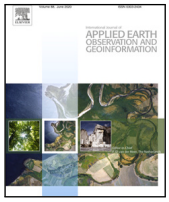

Global dynamics of the offshore wind energy sector monitored with Sentinel-1: Turbine count, installed capacity and site specifications

Thorsten Hoeser [a,*], Claudia Kuenzer [a,b]

[a] German Remote Sensing Data Center (DFD), German Aerospace Center (DLR), Muenchener Strasse 20, 82234 Wessling, Germany
[b] Department of Remote Sensing, Institute of Geography and Geology, University of Wuerzburg, Am Hubland, 97074 Wuerzburg, Germany

ARTICLE INFO

Keywords:
Offshore wind farm
Offshore wind energy
Renewable energy
Offshore infrastructure
Earth observation
Sentinel-1

ABSTRACT

With the promotion of renewable energy production and a planned phaseout of fossil fuels until 2040, the offshore wind energy sector has expanded and will continue to increase its capacity in the upcoming decades. This study presents a novel approach to deriving the installed capacity of offshore wind turbines on a global scale from spaceborne radar imagery provided by the Sentinel-1 mission. This new method contributes significantly to the information depth of freely available data sets, which provide the spatiotemporal patterns of offshore wind turbines. Furthermore, by combining freely available Earth observation and GIS data, commonly reported attributes of the offshore wind energy sector are compiled to provide a first impression of how this data can be used. All attributes are investigated to provide an in-depth overview of the developments in the offshore wind energy sector over the last five years. Between July 2016 and June 2021, the installed capacity worldwide grew from 13.5 GW to 40.6 GW. This corresponds to an increase of 27.1 GW or 200%. In total 8885 OWTs were installed until June 2021 with an additional 852 under construction. The European Union (15.2 GW), China (14.1 GW) and the United Kingdom (10.7 GW) are the three major contributors to the offshore wind energy sector. China has seen the largest growth in the last five years of 13 GW, followed by the EU with 8 GW and the UK with 5.8 GW. The provided analysis at the end of this study describes the offshore wind energy sector in a transition phase between decades of maturity and massive growth at a time when carbon-neutral energy production is massively supported. Overall the proposed approaches for independent offshore wind turbine capacity estimation and spatiotemporal investigation of the offshore wind energy sector can be used by all stakeholders involved in the upcoming challenge of integrated planning and implementation of offshore wind energy projects.

1. Introduction

In the Climate Pact of the 26th UN Climate Change Conference (COP26) in 2021, 65 countries agreed to massively decrease the use of fossil fuels for energy production with a coal phaseout until 2040 (COP26, 2021a). Another agreement urges the transition to zero-emission vehicles, pointing out the necessity of rapid progress in charging infrastructure and enabling the electrical grid for the increasing demand for electric vehicles (COP26, 2021b). These two goals are exemplary for a long-term carbon-neutral society: Energy production based on fossil fuels has to phase out while the demand for electrical power by new, carbon-neutral technologies increases. Electrical power generation has to change and expand simultaneously to achieve both goals. Therefore, a major contribution to future energy production in carbon-neutral societies will be a massive increase in renewable energy.

The offshore wind energy sector has grown steadily since 1991 and has become an important contributor to a carbon-neutral energy mix (Rodrigues et al., 2015). With the current promotion of renewable energy, there will be a massive expansion in the upcoming decades. In 2021, the UK government introduced the Net Zero Strategy, which targets to increase its offshore wind energy capacity from 10.5 GW in 2020 to 40 GW by 2030 (UK Gov., 2021). With an investment of EUR 800 billion, the EU announced expanding its offshore wind energy capacity from 12 GW in 2020 to 60 GW in 2030 and up to 300 GW in 2050 (EC, 2020). These two strategies will mainly affect the North Sea Basin. However, with an already ongoing and worldwide most extensive expansion in China and recently started constructions in the United States, the South and East China Sea and the US Atlantic coast are further examples demonstrating the global scale of the offshore wind energy expansion (Rodrigues et al., 2015). Thus, offshore wind

* Corresponding author.
E-mail address: thorsten.hoeser@dlr.de (T. Hoeser).

https://doi.org/10.1016/j.jag.2022.102957
Received 20 April 2022; Received in revised form 28 July 2022; Accepted 1 August 2022
Available online 11 August 2022

energy infrastructure deployment in marine space will increase dramatically. Today, many stakeholders are involved, and legal, economic, and ecological conflicts have to be considered along with the urgent task of deploying carbon-neutral energy infrastructure (Gusatu et al., 2020). Therefore, public access to independent information and ongoing monitoring of the offshore wind energy sector is crucial. With the proposed approach for offshore wind turbine (OWT) installed capacity estimation from freely available Sentinel-1 data, this study contributes to adding this most important metric to freely available offshore wind energy data sets, which describe the spatiotemporal patterns of single OWTs, but not their capacity.

Recent developments in image processing, especially from the deep learning domain (Zhu et al., 2017; Ma et al., 2019; Hoeser and Kuenzer, 2020), and free access to remote sensing data enable users to extract small-scale single object entities in large-scale Earth observation archives (Hoeser et al., 2020). Recently, Hoeser et al. (2022) introduced the DeepOWT data set, a global data set of offshore wind energy infrastructure which provides single OWT locations along with their deployment stages between 2016 and 2021, based on Earth observation data. In this study, the DeepOWT data set is employed to model the installed capacity of offshore wind turbines on a local to global scale and conduct an in-depth investigation of key attributes of the offshore wind energy sector over the last five years. Therefore, new data, which highly increases the information depth of the spatiotemporal DeepOWT data set, is derived from freely available Earth observation images. Thus, this application of Earth observation and geoinformation is an example of how the data and techniques from these domains can be used to investigate the current developments in the offshore wind energy sector.

2. Related research

Studies of detecting persistent marine infrastructure with Earth observation data have been carried out to provide data that can be used to investigate the human impact on marine ecosystems or to report the development of specific industries like oil production or offshore renewable energy. Radar remote sensing is specifically suitable since it is unaffected by clouds and offshore objects appear as bright backscatter clusters in front of the darker sea with a low backscatter coefficient. These imaging characteristics are commonly used to investigate offshore infrastructure. Wong et al. (2019) proposed a detection process based on the constant false alarm rate (CFAR) approach, which investigates preprocessed Sentinel-1 images by the difference of Gaussians (DoG) method to find object locations and further post-processing to weed out false positives. They deployed their algorithm on the Google Earth Engine and detected oil rigs in the Gulf of Mexico and offshore wind turbines in the exclusive economic zones of the UK and China. Zhang et al. (2021) processed the Sentinel-1 archive on a global scale and provided OWT locations by applying a morphological approach in combination with multiple thresholds to remove false positives. In addition to the spatial locations, the estimated first appearance of an OWT between 2014 and 2019 is provided in their study. Xu et al. (2020) investigated multispectral images from the Sentinel-2 and Landsat missions. To extract marine infrastructure, they used order statistic filtering in combinations with predefined thresholds. Combining the object candidates with existing vector geometries of offshore wind farms or human interpretation could further distinguish offshore wind energy infrastructure.

In a preceding study to this work, Hoeser et al. (2022) proposed the DeepOWT data set, which provides offshore wind energy infrastructure objects along with their deployment dynamics. Fig. 1 summarises how the DeepOWT data set was derived from Sentinel-1 images on a global scale. The Sentinel-1 acquisitions of the second quarter of 2021 were reduced to median composites on which a cascade of two convolutional neural networks (CNNs), optimised on fully synthetic training data (Hoeser and Kuenzer, 2022), detect offshore wind energy infrastructure. OWTs, transformer stations and platforms under construction were differentiated during the detection of the second CNN. The class differentiation is based on the investigation of the difference in spatial features which these classes represent, see Fig. 2. Based on the detected bounding box of an offshore infrastructure object, the multi-temporal deployment dynamics were derived by investigating changes in the local radar signature for a five-year stack of quarterly images. The final DeepOWT data set provides point locations which describe offshore wind energy infrastructure and their quarterly deployment stages from July 2016 until June 2021.

The reported studies mainly focus on improving spatiotemporal information. However, an important metric besides the location and deployment stage of an OWT is the installed capacity. As reported in Section 1, this metric is commonly used to inform about the size and development of the offshore wind energy sector and to communicate expansion goals of offshore wind energy strategies for the upcoming decades. Therefore, this study uses the spatiotemporal information provided by the DeepOWT data set to model this essential metric on a global scale based on Earth observation data.

Considering the achievements of related research, the contribution of this study can thus be divided into three aspects:

- The introduction to a newly developed radargrammetric approach for calculating the hub height of horizontal axis wind turbines (HAWTs) with subsequent statistical modelling of the installed capacity via the calculated height.
- The calculation of all turbine heights and corresponding installed capacities for all OWTs included in the global DeepOWT data set, based solely on Sentinel-1 data.
- A spatiotemporal analysis of the offshore wind energy sector from an Earth observation and geoinformation perspective, based on the enriched DeepOWT data set.

Fig. 3 highlights the benefits and contributions of the extended version of the DeepOWT data set proposed in this study by comparing it to other scientific and industrial global offshore wind turbine data sets. With the additional information on hub height and installed capacity at an OWT level, this extended version of the DeepOWT data set is the only existing data set, which is freely accessible and provides this depth of information on a global scale, see 3a). Furthermore, the DeepOWT data set provides the most spatially and temporally robust mapping performance compared to other freely available data sets, see 3b).

3. Data and material

This study uses the recently published DeepOWT data set due to its open accessibility, accurate spatiotemporal information and underlying Earth observation data, the Sentinel-1 archive. DeepOWT describes turbine locations with a quarterly time series from July 2016 until June 2021 along with the information if a turbine is under construction, readily deployed, or neither of both (Hoeser et al., 2022). Fig. 4 gives an impression of the data set, its global extent, two regional hot spots and a local example of turbine and transformer station locations for a large OWT cluster in the North Sea Basin. To further enrich the information for each single OWT location, the Google Earth Engine (GEE) (Gorelick et al., 2017) was used to query Sentinel-1 C-band radar data (Torres et al., 2012) for calculating the OWT height and installed capacity. Ground truth data of 50 OWT clusters regarding their hub height and the corresponding capacity in MW were acquired from publicly available sources, like OWF operator specifications, public planning documents or news portals, see the supplementary material in Appendix B. This data was used to validate the height calculation based on the Sentinel-1 images and to build the statistical model which links OWT height to OWT installed capacity. Moreover, the water depth from NOAA's ETOPO1 topography data set, available on the GEE, was also

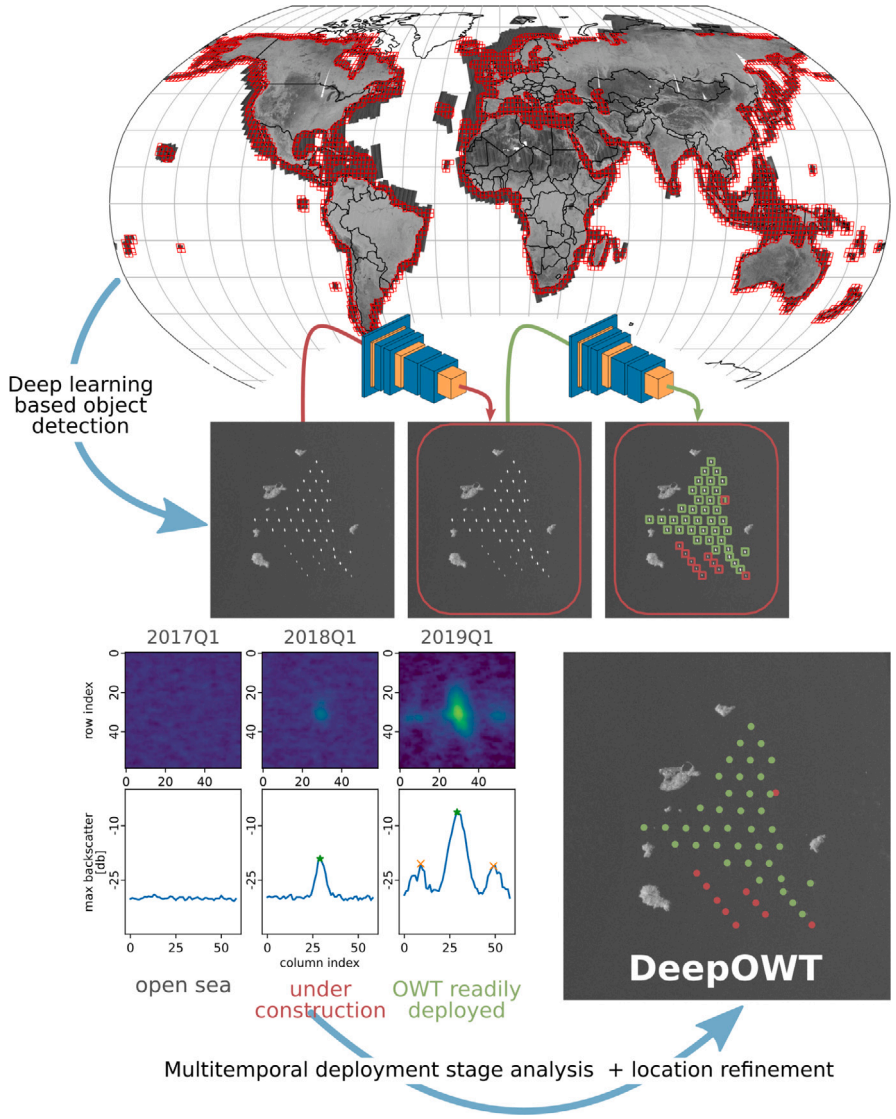

Fig. 1. Graphical summary of the workflow which has been used to derive the DeepOWT data set by Hoeser et al. (2022). Two convolutional neural networks analyse global Sentinel-1 data to find OWT locations. A time series from June 2016 until July 2021 is analysed for each OWT location to derive its deployment dynamics.

queried for each turbine location. ETOPO1 describes land topography and ocean bathymetry at a resolution of 1 arc minute on a global scale by combining multiple regional data sets (Amante and Eakins, 2009). Furthermore, the OWT locations from the DeepOWT data set are combined with vector data which describe the exclusive economic zones (EEZ) (Flanders Marine Institute, 2020) and the global coastline with minor islands (Natural Earth, 2022) to derive national affiliation and the minimum distance to the coast for each OWT, respectively.

4. Methodology

4.1. Installed capacity estimation

In order to design an independent and region agnostic estimation of the installed capacity, the workflow was based on freely and globally available Sentinel-1 data. Two steps were used to derive the installed capacity of an OWT from spaceborne radar imagery. In step one, the turbine's hub height is calculated by a radargrammetric investigation of the radar signature at an OWT location. In step two, a model links the calculated hub height to the installed capacity for each turbine.

4.1.1. Offshore wind turbine height calculation

Fig. 5(a) shows conceptually how the hub height of an OWT was calculated with Sentinel-1 data. A rectangular 400 × 400 m area was defined for each OWT location. For these areas, all Sentinel-1 acquisitions between April to June 2021 with the specification GRD (ground range detected), IW (interferometric wide swath), VH (vertical–horizontal polarised), ascending orbit and from a single platform A or B were stacked and reduced to a single band median composite. The example in Fig. 5 shows two main backscatter clusters. One large cluster in the centre at the detected location of an OWT and left to it, a smaller cluster. The smaller cluster to the left of the OWT appears due to the right-looking sensor geometry, and the layover effect (Meric et al., 2009) depicted in 5(b). The radar signal first hits the nacelle before hitting the larger foundation at sea level. Thus, when projected onto the ground range, the part of the signal that hits the nacelle gets distorted and appears in front of the undistorted centre location. Visually in the map-view, it looks like the turbine leans toward the sensor.

Furthermore, 5(c) and (d) describe how the resulting geometry can be used for height calculation. 5(c) describes how the local incident angle θ increases with increasing ground range. At the same time, α increases too, allowing to approximate a right angle between the

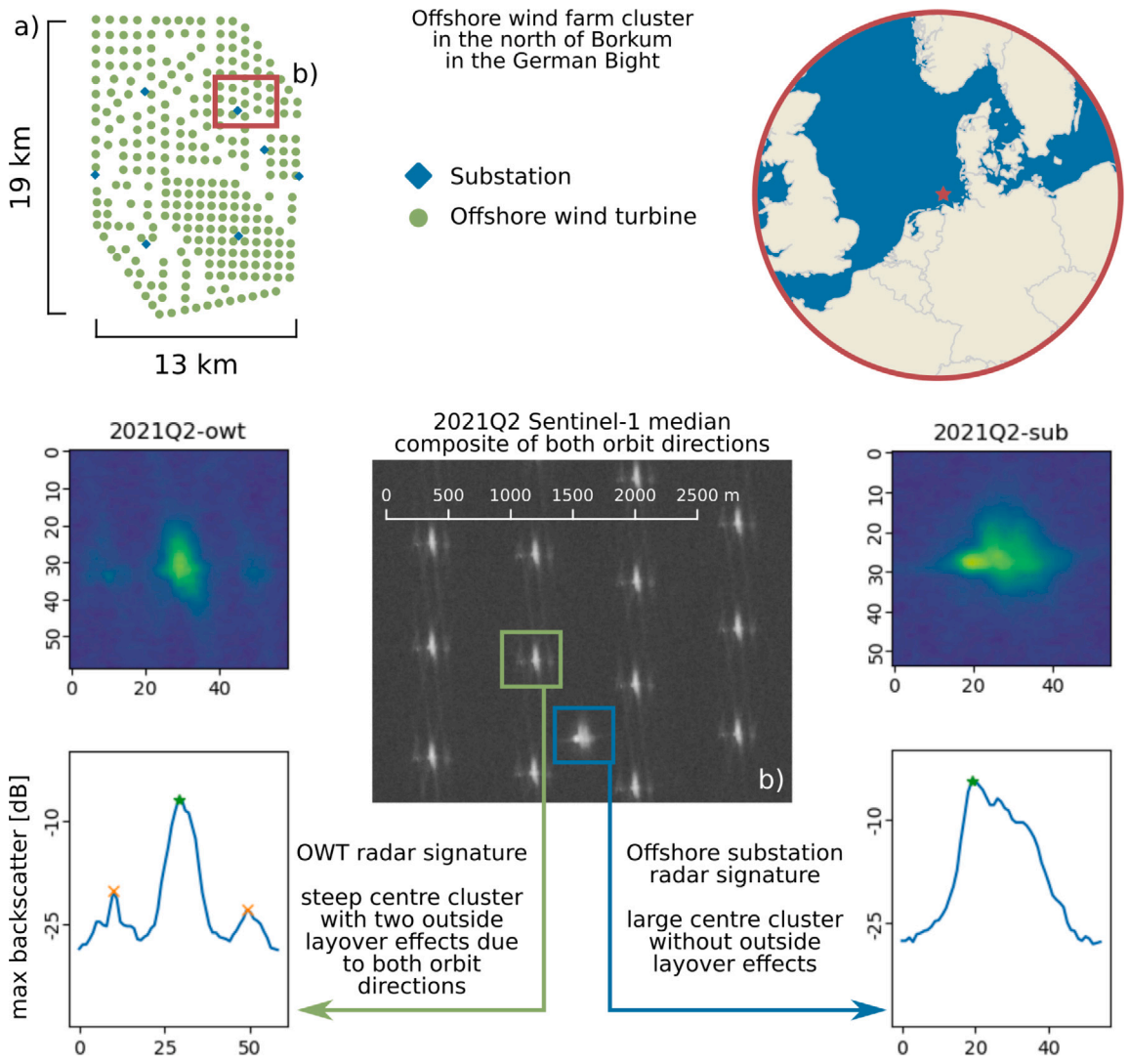

Fig. 2. Visualisation of different spatial features of offshore wind turbines and offshore wind energy substations in Sentinel-1 radar signatures as they occur in median composites, which are based on ascending and descending orbit directions. The employed CNN-cascade in Hoeser et al. (2022) uses these features to differentiate both classes during the generation of the DeepOWT data set.

theoretical hypotenuse of nacelle and layover cluster, and the radar signal with a local incident angle θ_{OWT} at the OWT location, see Fig. 5(d). It follows that α and θ_{OWT} are equal.

The incident angle θ_{OWT}, and thus α, is provided as a separate layer for each Sentinel-1 acquisition. For each OWT location, the corresponding incident angle is retrieved by querying the incident angle band of all Sentinel-1 acquisitions provided by the GEE, contributing to the quarterly median composite. In order to avoid different incident angles, in the case of locations where two neighbouring orbits overlap and to retrieve a single value for the height calculation, the stack of queried incident angles is reduced. Therefore, the incident angle with the most frequent occurrence, the mode of all incident angles, is selected from the quarterly stack of incident angles.

A theoretical right triangle can be constructed to calculate the hub height of the OWT, where the side opposite is the hub height, the side adjacent is the absolute distance between the centre cluster and layover cluster, and α is its corresponding angle. The layover cluster location was extracted by applying a peak finder algorithm on the maximum swath profile along the horizontal axis of the radar image, see 5(e). By reprojecting the coordinates of OWT and layover centre to their corresponding UTM coordinate system, the absolute distance between the points was calculated. The calculation of the side opposite was done cluster-wise for each OWT. Therefore, an OWT cluster was defined manually by its spatial proximity and OWT deployment date, provided by the DeepOWT data set. In order to reduce outliers of calculated height values, the median of all calculated heights within one cluster defines the final height for all OWTs of the same cluster.

For 50 OWT clusters, the calculated heights were compared to ground truth data. Fig. 6 shows that the variance of the calculated heights can explain 77% of the variance of the ground truth heights, and the mean absolute error is 6.45 m. Since the derived locations of OWT and layover cluster are the pixel centres in the Sentinel-1 image with a spatial resolution of 10 × 10 m, the side adjacent has a theoretical error ε_{adj} with a range between −10 and +10 m, see Fig. 7. The maximal contribution of this sub-pixel error to the absolute height error $\varepsilon h_{\varepsilon_{adj}}$ ranges from 6 m to 10.36 m depending on the local incident angle. For the Sentinel-1 IW GRD products, the near range angle is θ_{min} (31°), and the far range angle is θ_{max} (46°) (Torres et al., 2012). Thus the mean absolute error of 6.45 m of the calculated heights is within the range of the maximum error $\varepsilon h_{\varepsilon_{adj}}$ demonstrating the general practicality of the height calculation approach.

4.1.2. Installed capacity model

In order to model the installed capacity, the data set of 50 OWT clusters, for which hub height and nominal capacity were looked up in operator specifications and official planning documents, was randomly

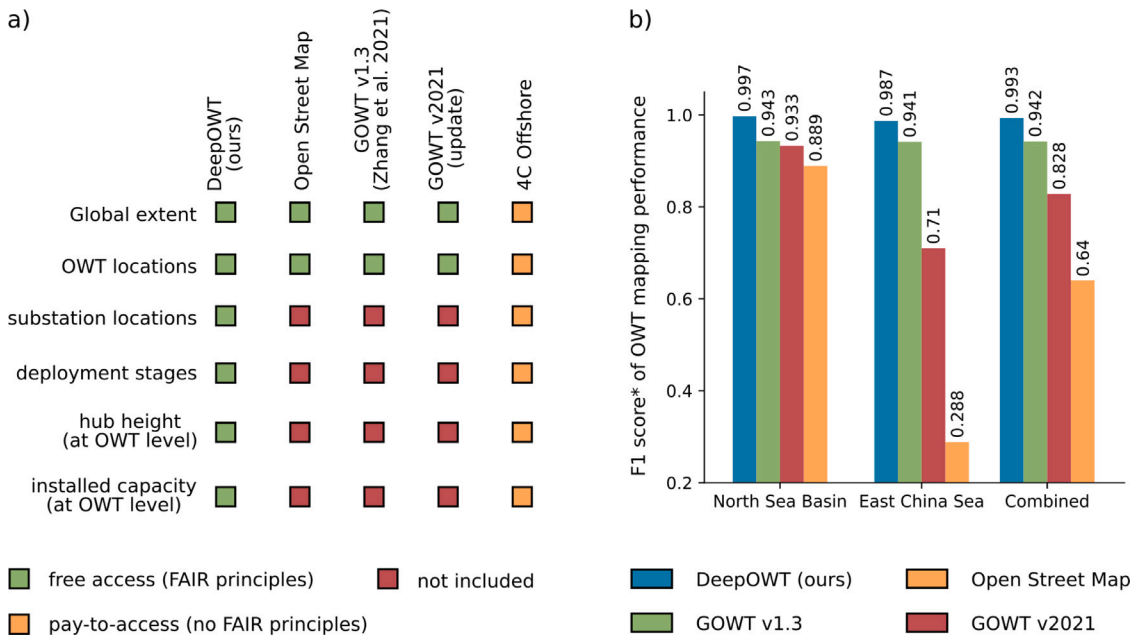

Fig. 3. (a) Qualitative comparison of content and accessibility of different offshore wind turbines (OWT) datasets from science and industry. (b) Quantitative comparison of OWT mapping performance of freely available datasets for the two ground truth test sites, the North Sea Basin and the East China Sea. *A detailed description of the methodological workflow for the calculation of the F1 scores, as well as all related scores for an in-depth comparison, can be found in Appendix A.

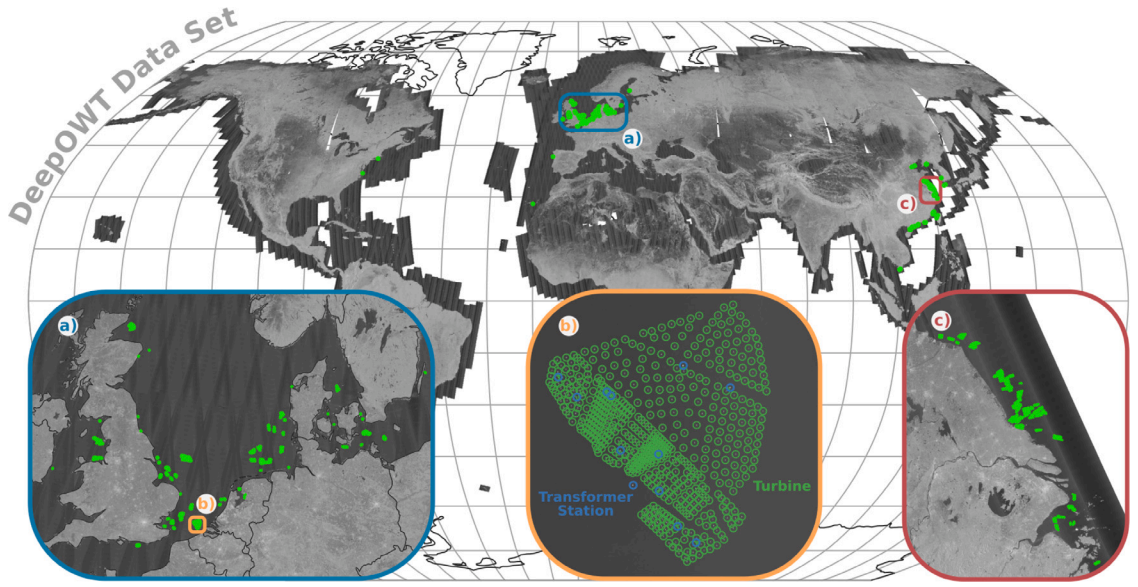

Fig. 4. Locations of offshore wind energy infrastructure, provided by the DeepOWT data set. The magnifications show (a) OWT clusters in the North Sea Basin, (b) a local close up of one large OWT cluster of the Netherlands and Belgium, and (c) OWT clusters in the northern East China Sea in June 2021.

split into a train and test data set with 36 and 14 entries, respectively. Fig. 8 proposes a correlation between hub height and installed capacity of a wind turbine for the train split. With this observation, the parameter *installed capacity* can be estimated using the calculated height as the independent variable. The hypothetical model h is a sigmoid function, see Eq. (1), in order to approximate logistic growth where L is the curve's maximum, k the logistic growth rate, x_0 the offset of the x-axis and b the offset of the y-axis.

$$h(x) = \frac{L}{1 + e^{-k(x-x_0)}} + b \tag{1}$$

The sigmoid function enables the modelling of logistic growth, which can be recognised in the first half of the training data between hub heights of 60 to about 95 m. However, the further progression beyond 95 m diverges from a purely logistic growth, with a higher variance and tendency to level off. Thus the second part of the sigmoid function supports modelling this part of the training data without overestimating higher heights.

The parameters of the hypothetical model are optimised by minimising the least-squares cost function on the train data, resulting in the fitted model shown in Fig. 8 and its corresponding 95% confidence interval (CI). The optimised model was used to predict the installed capacity for each OWT based on the calculated heights. The predictions were compared to the test and also the train OWT clusters. The corresponding error distribution of test and train split were compared by a Kolmogorov–Smirnov (KS) test (Smirnov, 1939) with a significance level of 0.05. The KS test confirmed the null hypothesis with $p = 0.09$, that both distributions are identical, see Fig. 9. Thus, the train and test split are combined in the following error discussion.

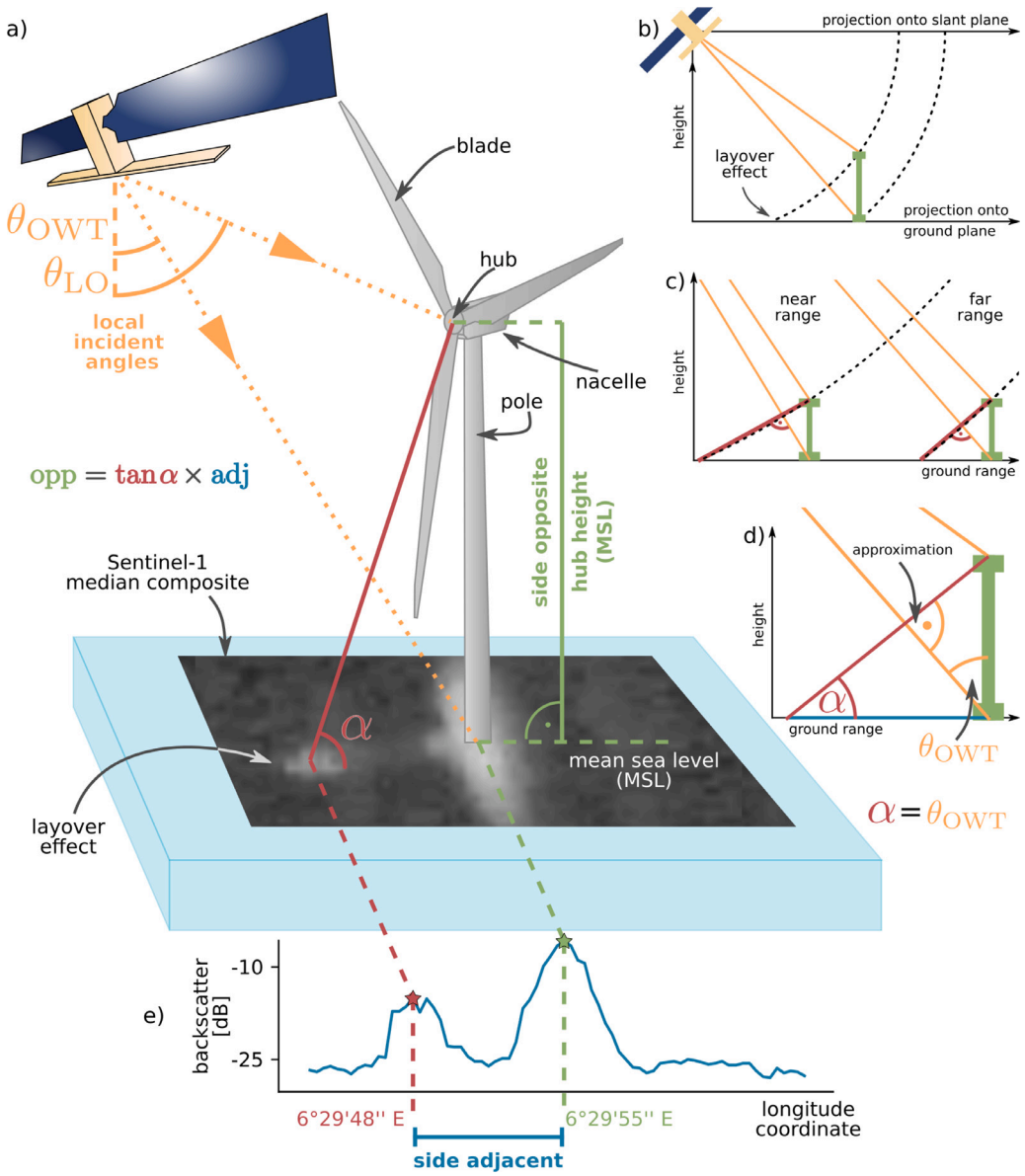

Fig. 5. Conceptual visualisation of calculating the hub height of an offshore wind turbine by investigating the layover effect caused by the imaging geometry of the Sentinel-1 radar instrument and the target object.

Fig. 9 shows that the variance of the estimated installed capacity can explain 90% of the variance of the ground truth capacity. Furthermore, the error follows a normal distribution with a mean at 4.76 MW close to 0. Thus, no systematical error was observed, which tends to always over or underestimate the installed capacity. The mean absolute error is 36.16 MW, less than 15% of the mean installed capacity of the ground truth data of 244.98 MW. For a large-scale comparison of the model predictions on more than the 50 OWT clusters, we refer to Section 5, where region-based capacities from different sources are compared with the installed capacity estimations in this study.

4.2. Deriving commonly reported attributes

To further enrich an OWT location besides its hub height and installed capacity, more attributes commonly reported in the wind energy sector to describe an offshore wind farm or turbine were derived by spatial queries and geoprocessing.

4.2.1. Offshore wind turbine distance to coast and nearest neighbour

The two characteristics, distance to the nearest OWT and minimum distance to shoreline, were added for each OWT. Before the distance was calculated, every data set used in these processes was reprojected to each OWT location's corresponding UTM coordinate reference system (CRS). No auxiliary data was necessary to calculate the minimum distance between OWTs. Fig. 10 shows a pattern of the resulting distances in a European offshore wind farm cluster. This visualisation shows a trend of increasing turbine distance over time due to the installation of OWT with larger rotor diameters.

For the OWT to shoreline distance, a detailed coastline including minor islands was used as the target polygon (Natural Earth, 2022). In order to minimise the processing effort, for each OWT location, the global data set was clipped with a 200 km radius around the OWT location before searching for the smallest OWT to shoreline distance. Similar to the nearest OWT distance, the distance to the shoreline increases over time for the local example of the east England coast, shown in Fig. 11. The Hornsea Project, also visualised in this figure, is the furthest offshore wind farm project from the mainland, partly deployed in 2021.

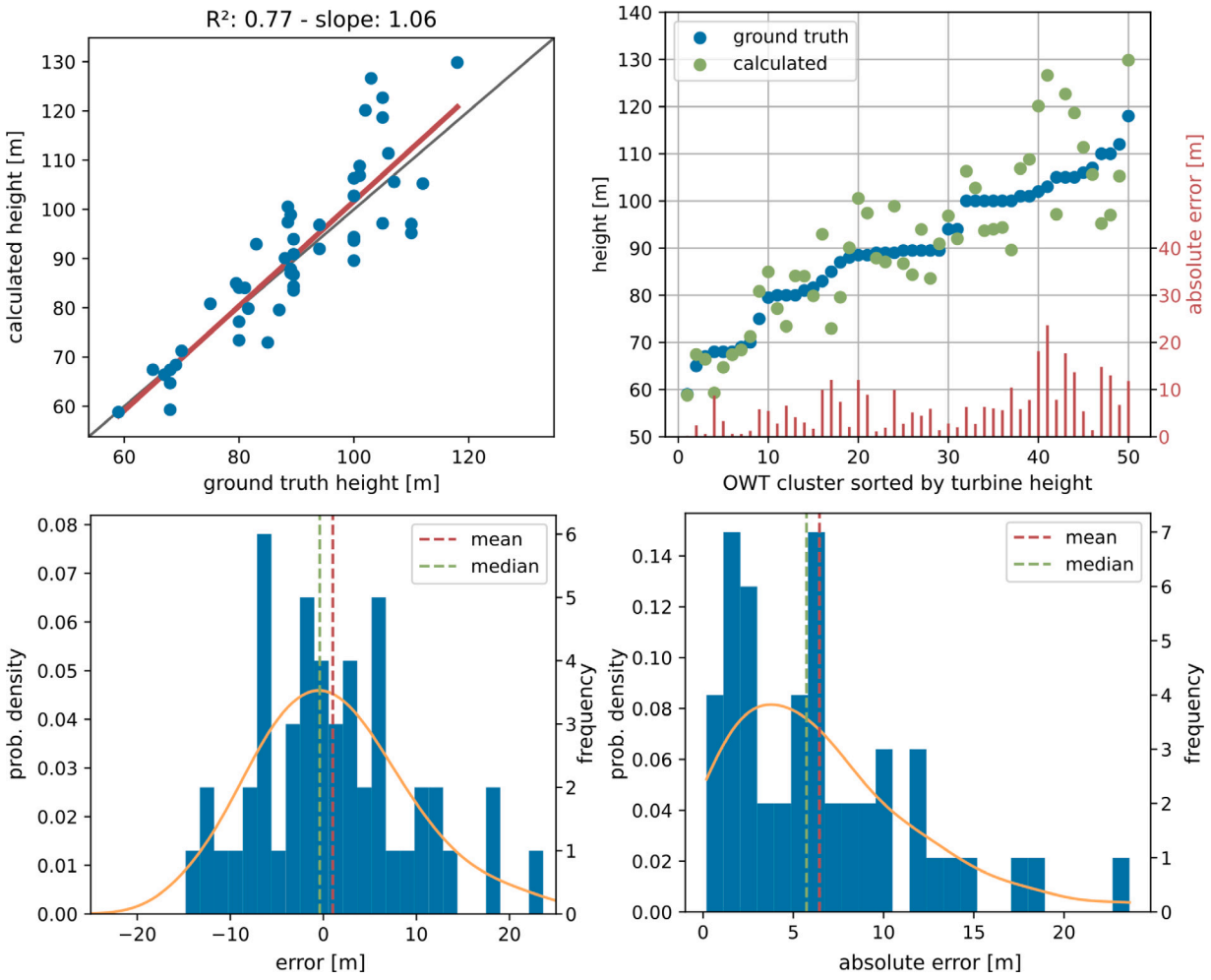

Fig. 6. Error discussion of the calculated offshore wind turbine hub heights. The upper row shows the correlation between predicted and ground truth heights and the residuals. The lower row shows the distributions of the error and absolute error.

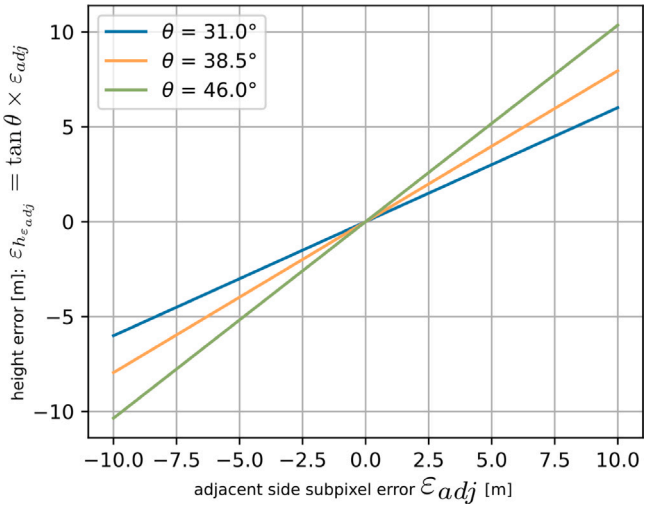

Fig. 7. Boundaries of the theoretical contribution to the hub height error caused by location inaccuracy due to the spatial resolution of 10 m and incident angle of the Sentinel-1 sensor. Thereby, the near range incident angle is 31° and the far range incident angle is 46°.

4.2.2. Offshore wind turbine water depth and national affiliation

For the last two attributes, the water depth at an OWT location and the national affiliation, spatial queries are used to obtain the information. The water depth was obtained from NOAA's ETOPO1 data set (Amante and Eakins, 2009) via the GEE by using OWT locations provided by the DeepOWT data set. Fig. 12 shows the bathymetry component of the ETOPO1 data set for the two wind energy production hotspots, the North Sea Basin; and the northern East China Sea and the Yellow Sea. Both sites show large areas with relatively shallow waters close to the coast, which is one crucial factor for cost-efficient offshore wind turbine deployment. For the European Union, the difference in areas with a shallow water depth of the North Sea Basin compared to the Atlantic Ocean and large parts of the Mediterranean Sea is striking, and one explanation why nearly all OWFs of the EU are installed in the North Sea Basin and Baltic Sea.

The national affiliation was queried by applying a spatial join with the DeepOWT data set and the geometries of the national exclusive economic zones (EEZ) Flanders Marine Institute (2020). This completes the information enrichment of the DeepOWT data set. Six commonly used attributes for describing offshore wind farm projects (Rodrigues et al., 2015) have been added to the DeepOWT data set by combining methods from Earth observation, geoinformation and statistics.

5. Spatiotemporal evolution of turbine count and installed capacity

By combining the DeepOWT data set with further investigations of Sentinel-1 data, it was possible to provide installed wind energy

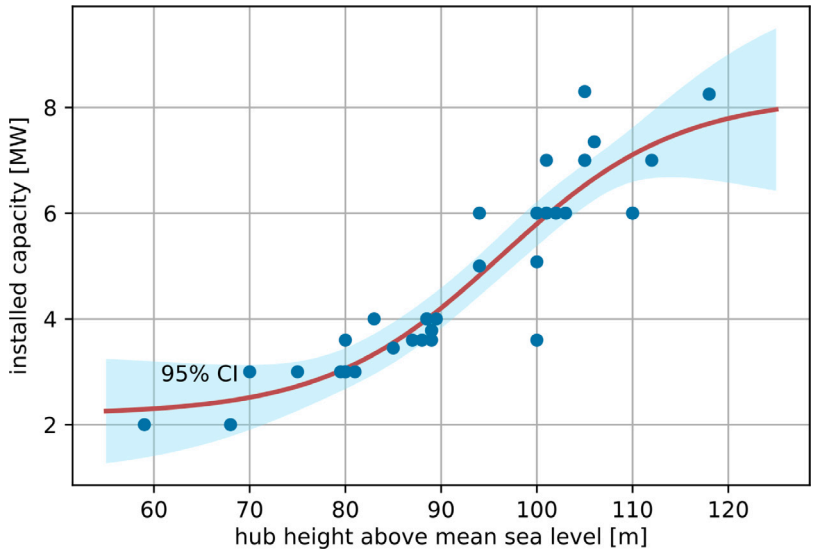

Fig. 8. Training data and fitted sigmoid function with its corresponding 95% confidence interval (CI) to map an offshore wind turbine's hub height to its installed capacity.

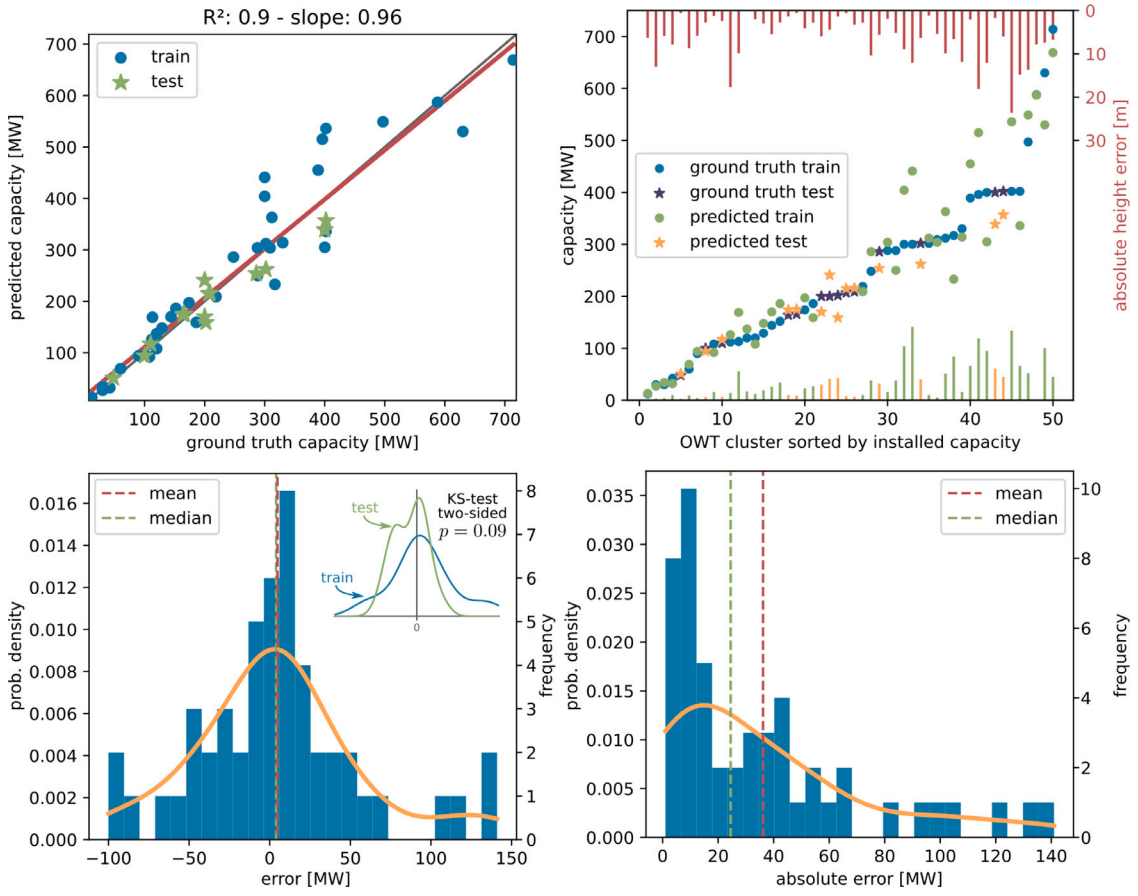

Fig. 9. Error discussion of the estimated offshore wind turbine installed capacity. The upper row shows the correlation between predicted and ground truth installed capacity and the residuals. The lower row shows the distributions of the error and absolute error.

capacity estimations based on this single Earth observation mission. In June 2021, the cumulative installed capacity of 8885 offshore wind turbines was 40.6 GW for the entire Earth. This corresponds to an increase of 27.2 GW or 200% realised by 5268 OWTs deployed within five years. Fig. 13 shows that mainly three big players dominate the offshore wind sector: The European Union, the People's Republic of China and the United Kingdom, sorted by installed capacity. Despite one of the worldwide largest onshore wind capacities in the United

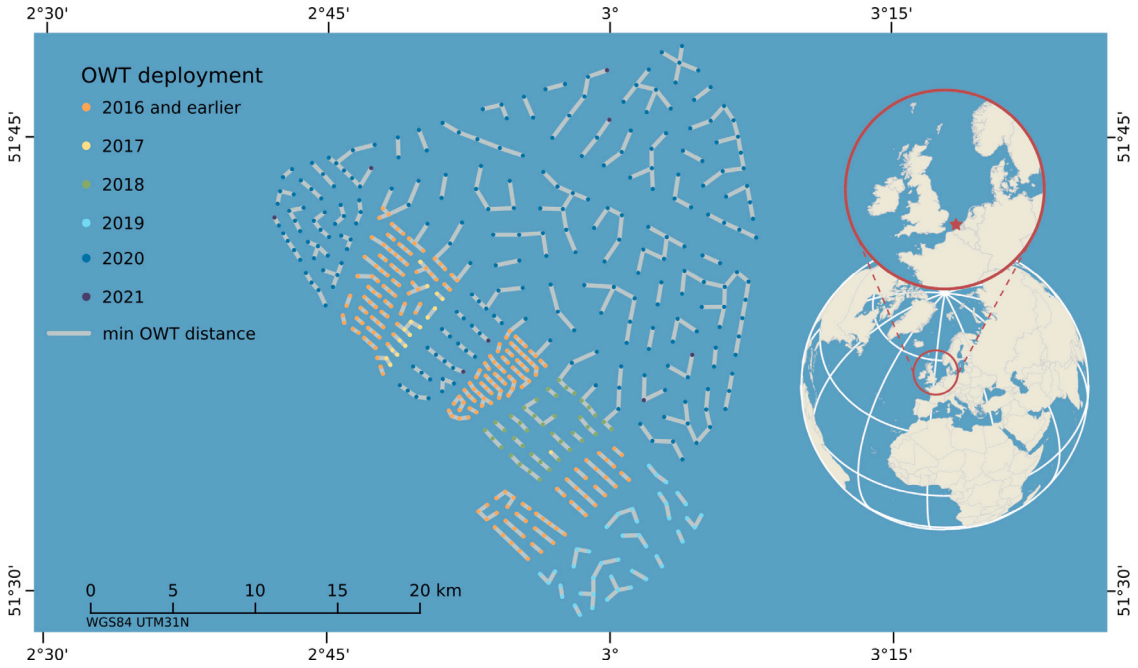

Fig. 10. An Offshore wind farm (OWF) cluster in the exclusive economic zones of the Netherlands and Belgium. The temporal dynamic indicates a trend of an increasing distance between single turbines.

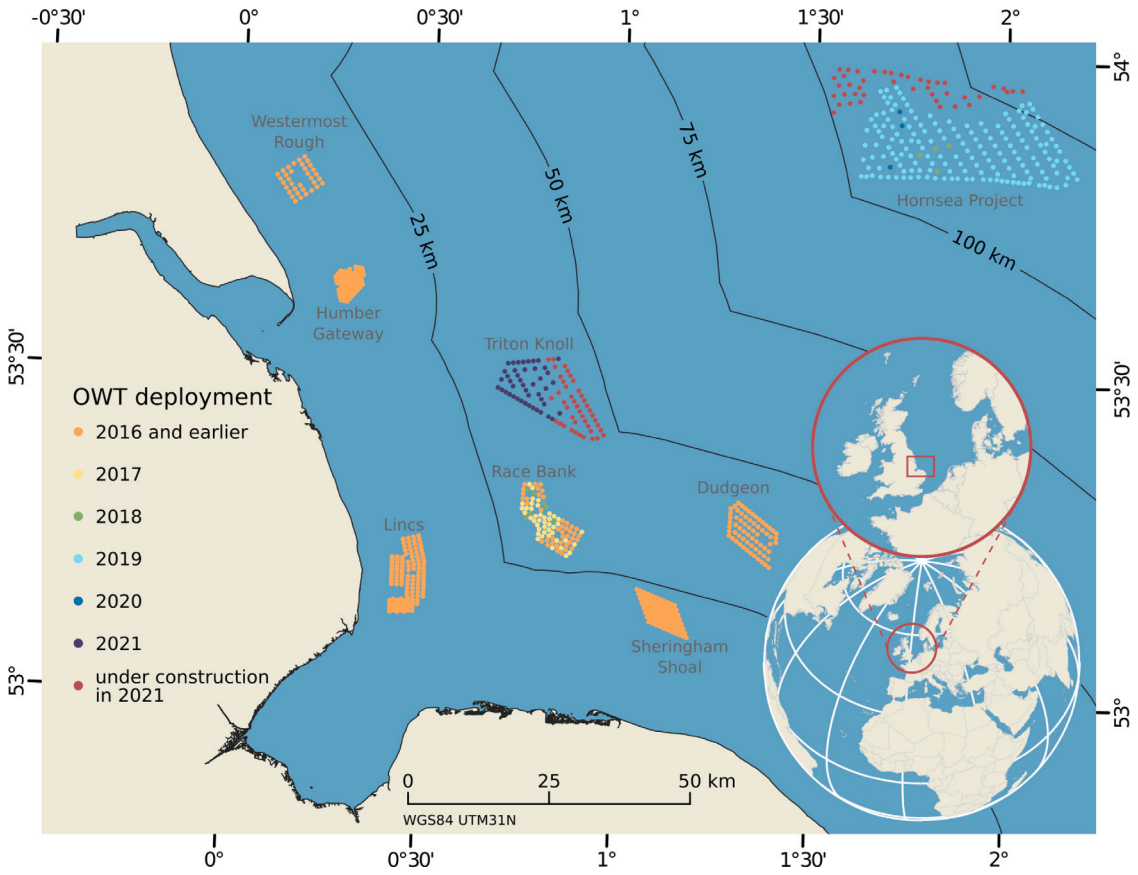

Fig. 11. Offshore wind farms (OWF) and their single turbine locations at the East England coast in the North Sea Basin. The temporal dynamic indicates an increasing distance between OWF projects and the shoreline.

States of America, offshore wind energy is early, with pilot projects and only seven installed OWTs. However, recently construction work has started for large-scale offshore wind farms on the Atlantic coast, and new sites are under development in this region.

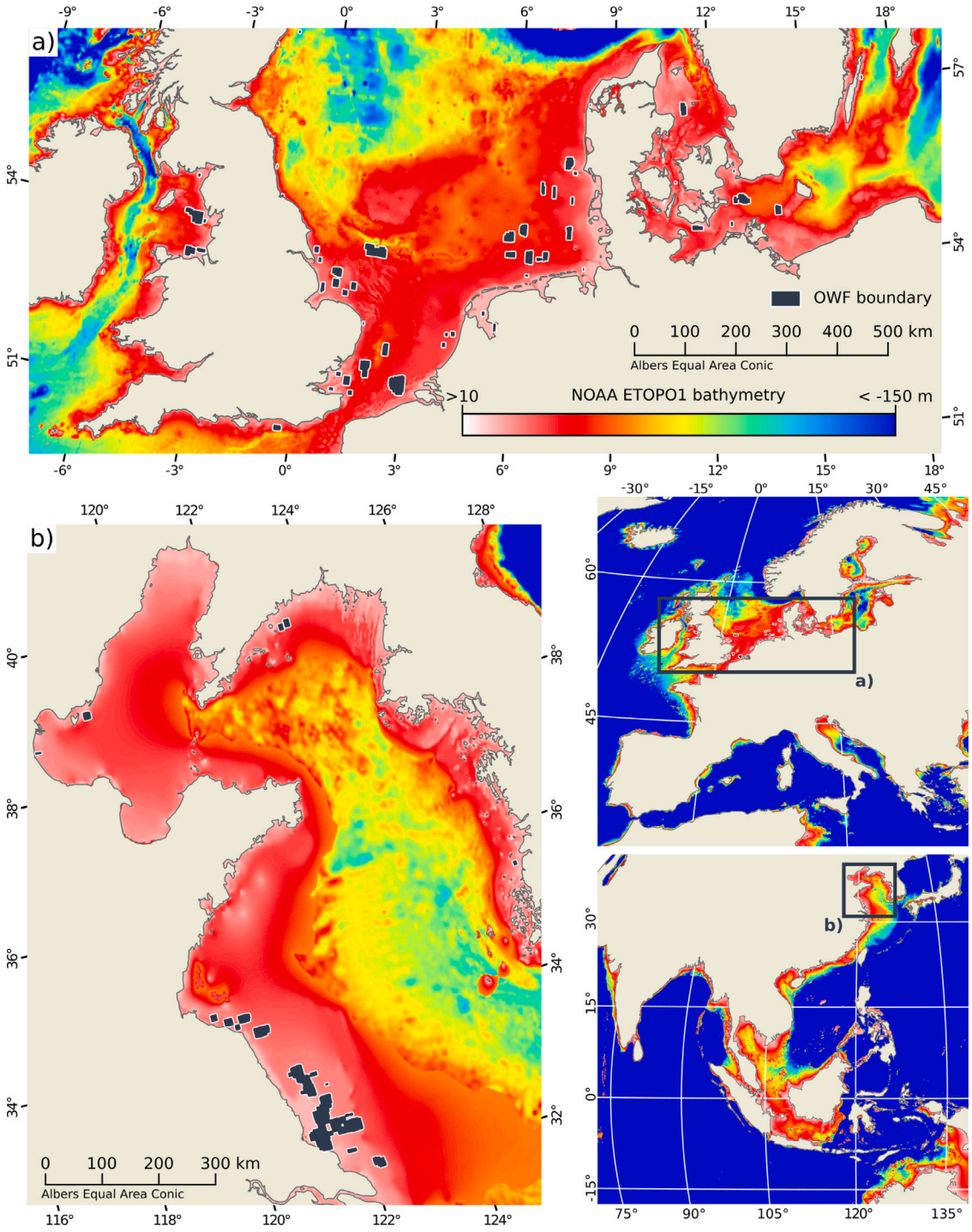

Fig. 12. Bathymetry of (a) the North Sea Basin and Baltic Sea and (b) the northern East China Sea and the Yellow Sea. Both sites show large areas of shallow water depth of about 50 m or less near the coast, which is an important factor for offshore wind farm deployment.

Fig. 13 already suggests recently high deployment dynamics in China with the most wind turbines built and under construction worldwide, which is confirmed in Fig. 14. In the last five years, China has had the highest increase in both installed capacity and the number of installed OWTs. Fig. 15 provides in-depth insight into the temporal deployment dynamics from July 2016 until June 2021. For China, it shows that the onset of offshore wind turbine deployment took place about five years ago and that within the last five years, the global trend of the offshore wind energy sector was greatly influenced by the deployment of 2960 OWTs with a cumulative capacity of 13 GW. By finishing the planned projects with 627 OWTs under construction in June 2021, in 2022, China will lead in the number of readily deployed OWTs and installed offshore wind turbine capacity worldwide. In comparison, the EU and UK already had numerous offshore wind farms back in 2016, originating from the initial Danish offshore wind farm project Vindeby in 1991 with 5.5 MW and developed the offshore wind sector to maturity over the last decades (Rodrigues et al., 2015). Since 2016, the number of OWTs and installed capacity increased by 1313 OWT and 8 GW, and 916 OWT and 5.8 GW for the EU and UK, respectively. In the upcoming decades, EU's (EC, 2020) and UK's (UK Gov., 2021) offshore wind programmes will lead to a surge of offshore wind farm projects. Together with China's recent and ongoing contribution, the

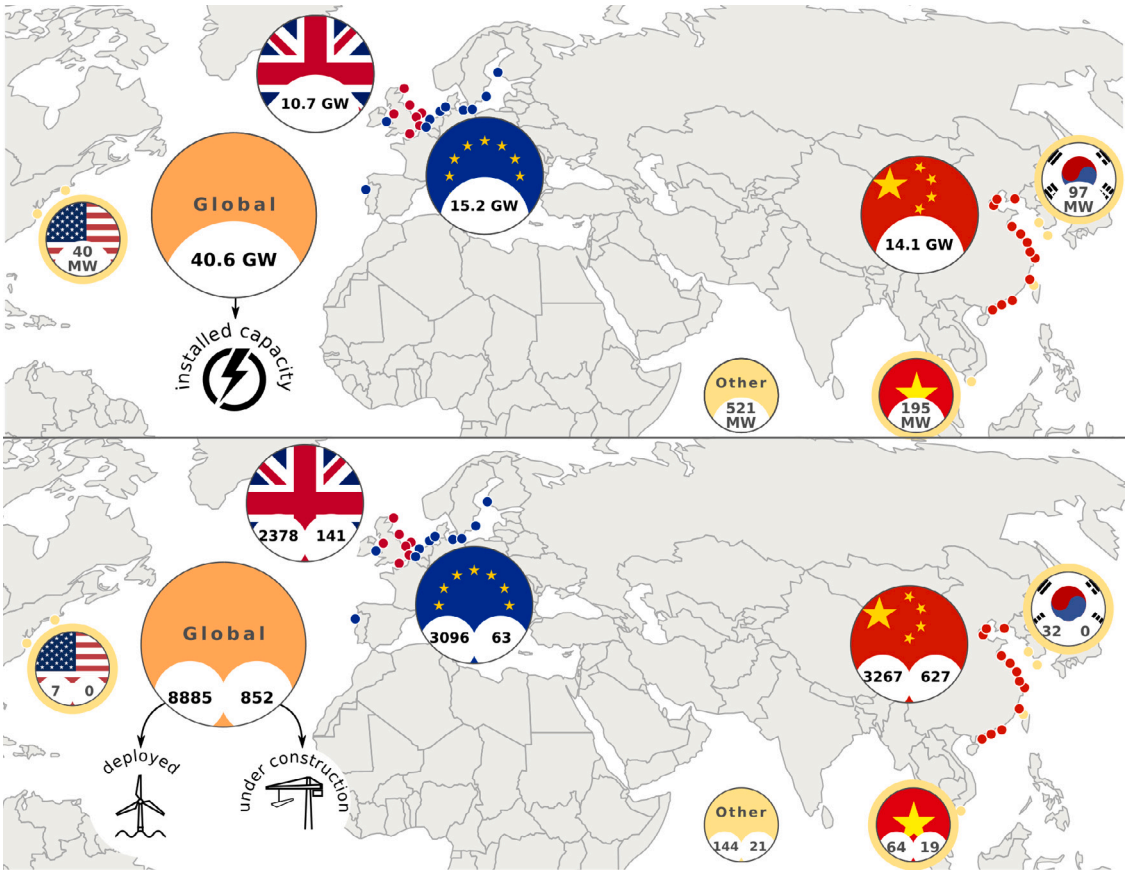

Fig. 13. Global distribution of offshore cumulative installed capacity (upper part), and the number of offshore wind turbines, readily deployed and under construction (lower part) by the end of June 2021. Single points in the maps indicate clusters of offshore wind farm projects. The three major offshore wind energy sector contributors are the EU, China and the UK. Further contributors are aggregated to the group "Other" referred to in the proceeding analysis.

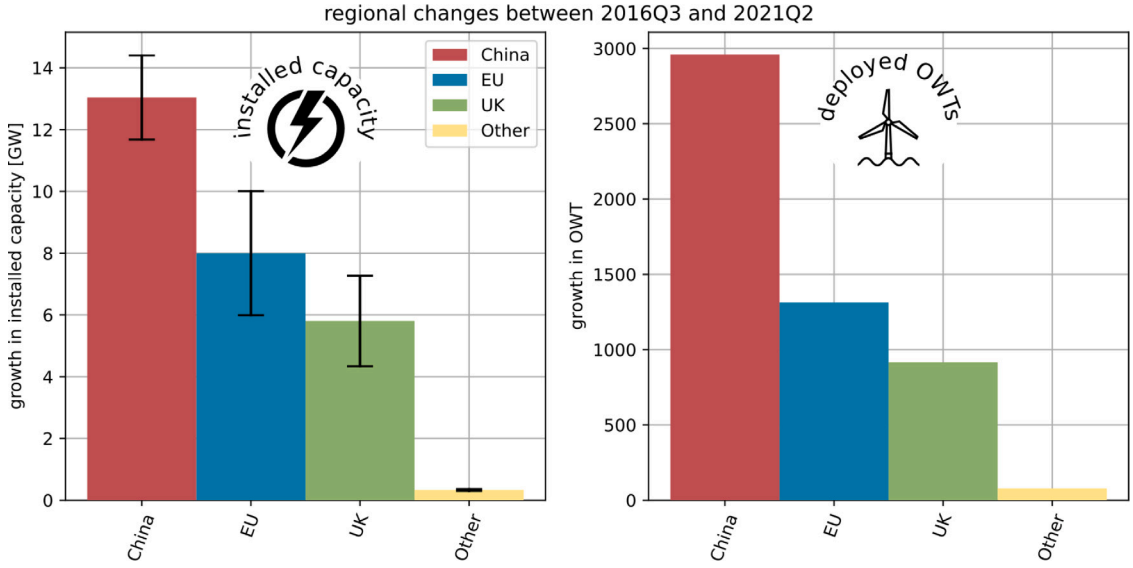

Fig. 14. Absolute changes in installed capacity (left) and the number of readily deployed offshore wind turbines (OWT) (right) within five years from July 2016 to June 2021, aggregated by region. The error bars for installed capacity indicate the standard deviation of the model used for the estimation.

start of construction work of large-scale offshore wind farms in the US and other nations joining the offshore wind energy sector, these developments will further contribute toward carbon-neutral energy production on a global scale.

This study's reported number of installed capacity solely relies on investigations of Earth observation data, as presented in Section 4.1. The installed capacity for 2020 is 35.149 GW on a global scale. This value is 0.144 GW below the official value of 35.293 GW for 2020 published by the Global Wind Energy Council (GWEC), whose annual reports can be assumed to be the strongest baseline. Fig. 16 provides a comparison of the derived installed capacity and number of turbines with several official reports. The estimated installed capacity

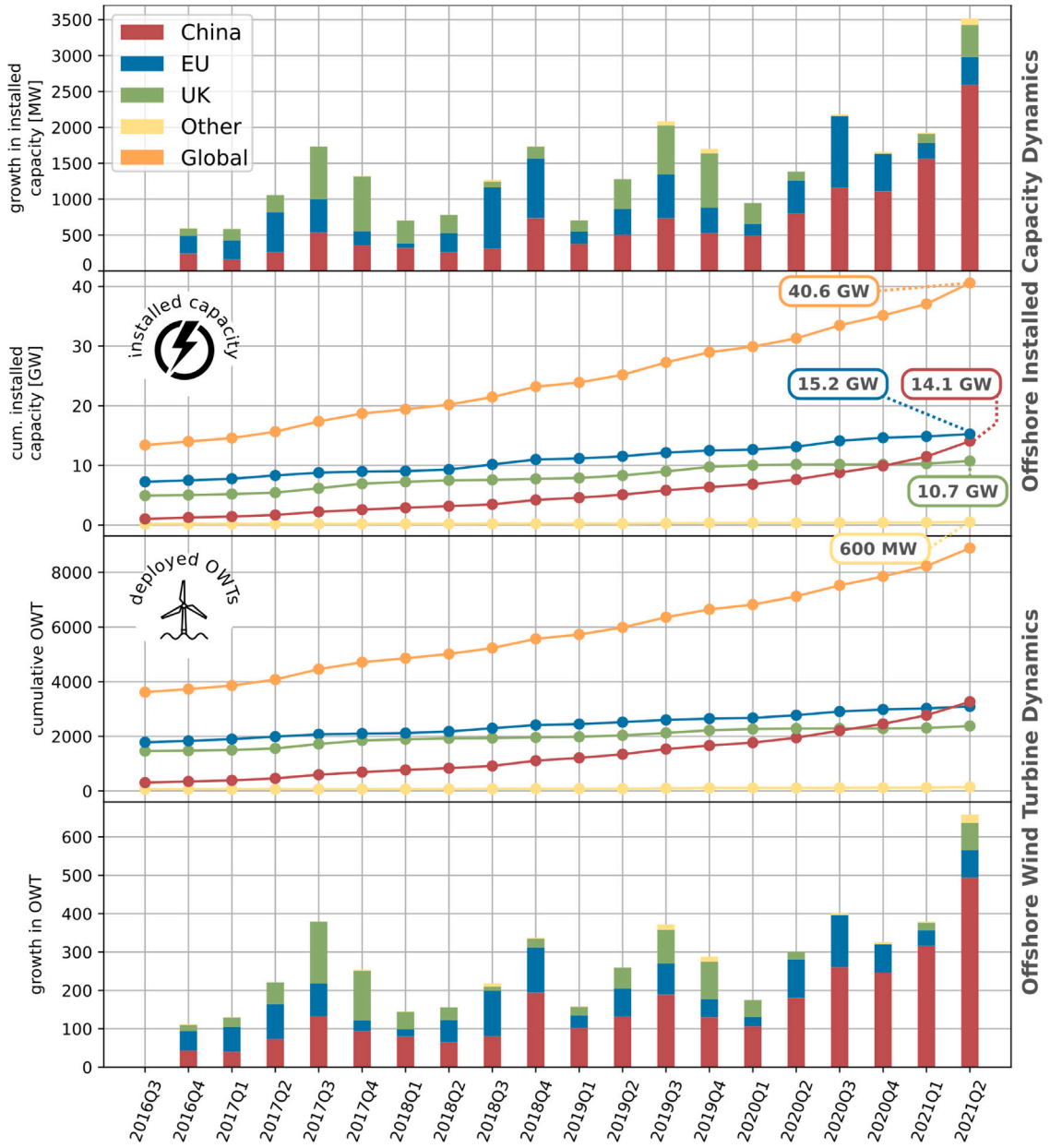

Fig. 15. Temporal dynamics of the installed capacity (upper part) and the corresponding number of offshore wind turbines (lower part) aggregated by regions. The time series shows the quarterly evolution over five years between July 2016 and June 2021.

and number of OWTs reported in this study are largely confirmed by these reports and can even provide consistently annual numbers. This demonstrates that freely available Earth observation data, combined with the proposed analysis techniques, can independently monitor the global dynamics of the offshore wind energy sector. Furthermore, the small-scale resolution based on individual turbines allows a fast and individual aggregation of units in space and time in order to examine developments in detail. This is impossible by using the public reports mentioned above since they only provide aggregated information. The following analysis of the attributes compiled in this study gives an impression of how trends in the offshore wind energy sector can be analysed by flexibly aggregating information in time and space.

6. Spatiotemporal evolution of site specifications

Fig. 17 provides an overview of temporal dynamics on a global scale and differences between the major offshore wind energy-producing regions for all investigated attributes. Installed capacity and hub height show similar trends and regional characteristics for the same investigation units. The quantile regression trend lines show that fewer small OWT units of nominal capacity and hub height were installed over the last five years. Nevertheless, at the same time, the trend for larger OWT units is not that clear yet. When looking at regional comparisons and keeping the deployment dynamics of the last five years in mind, it becomes clear that the surge of installed OWTs in China was characterised by OWTs with medium hub height and nominal capacity, about 4 MW, compared to such in the EU or UK. This explains why China has more OWT units than the EU, but the EU still had a higher amount of installed capacity in June 2021, see Fig. 13. Since China's contribution to the temporal dynamics has been the most influential over the last five years, the Chinese signal subdued the trend of larger OWT units on a global scale. However, when looking at the regional comparison, the EU and UK have already started building larger OWTs with higher nominal capacities, a trend that will continue.

The third row of Fig. 17 shows the development of the minimum distance to the shoreline. The global temporal trend appears to be

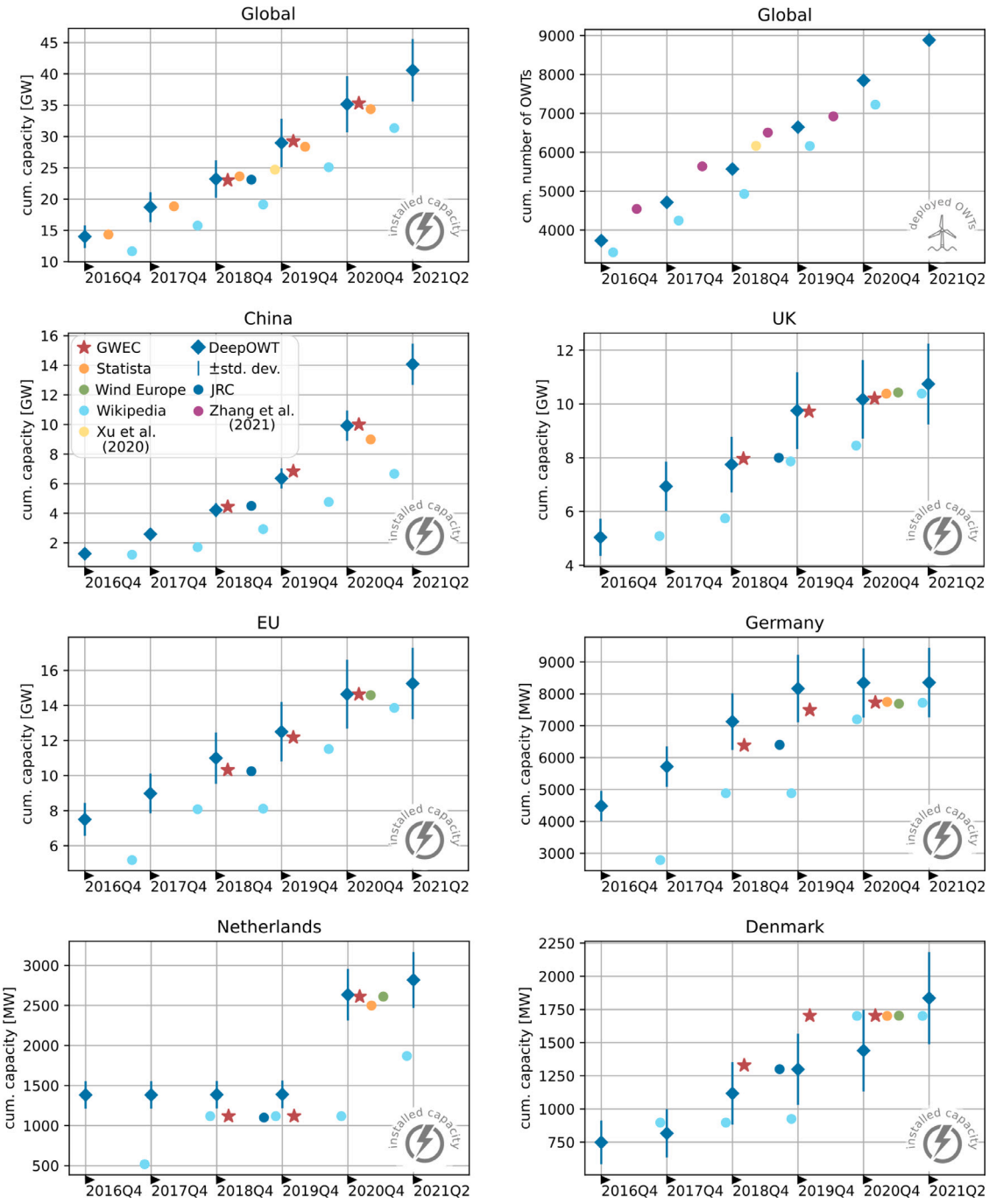

Fig. 16. Comparison of the derived installed capacity and number of turbines to official reports, public data, and scientific publications: Statista (Statista, 2021b,a), Global Wind Energy Council (GWEC) *strongest baseline (Lee and Zhao, 2020, 2021), Wind Europe (Ramírez et al., 2021) and European Commission Joint Research Centre (JRC) (European Commission et al., 2019; Wikipedia, 2022; Xu et al., 2020; Zhang et al., 2021).

mixed and less distinct due to regional peculiarities for this attribute. Most of the OWTs in China are built very close to the shoreline, whereas in the EU, and lately, in the UK, OWTs are built further away from the coast, resulting in a mixed global trend. However, for China and the UK, the temporal trends are clear. New OWTs are getting constructed with increasing distance to the coast. For example, in 2019 the first phase of the Hornsea Project was finished 120 km from the North East coast of England, which can clearly be seen even in the global trend in 2019Q2–2019Q4. More projects with increasing distance to the coast are planned in the EEZ of the UK where shallow waters are available far off the coast, like the Dogger Bank, where the Dogger Bank Wind Farm will be realised in the upcoming years with a maximal distance to the shoreline of about 290 km. The necessity of increasing distance to the shoreline indicates that capacities have already been exploited for a specific region near the shore. For the UK and China, this is a continuously progressive process. For the EU, single EEZs of its members are very different in shape and bathymetry. Thus, it appears to be that no general trend exists. Here, it would be interesting to look at a national scale to see how much of its nearshore capacities each EU member already has used and which bathymetry characteristics are generally prevalent.

The nearest neighbour distance between OWTs shows an increase for higher values, indicating that OWT units with larger rotor diameters that need larger distances to the next OWT are getting installed, which

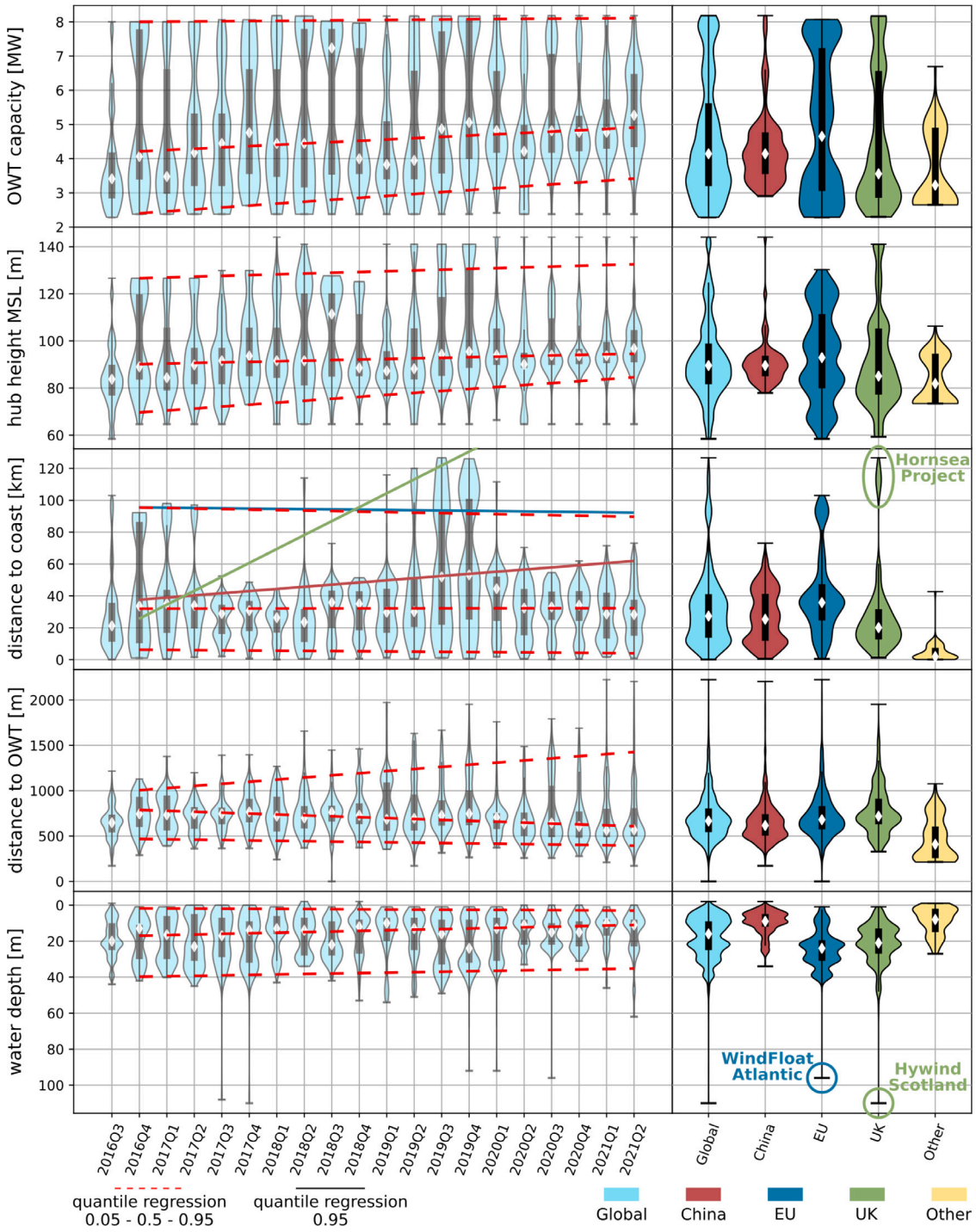

Fig. 17. On the left side are the temporal dynamics between July 2016 and June 2021 of the offshore wind turbine (OWT) related attributes on a global scale. The dashed trend lines show the 0.05–0.5–0.95 quantile regressions. For the attribute distance to coast, the 0.95 quantile regression for the EU, UK and China are provided separately. On the right side, the same attributes are aggregated by regions for the entire period.

was already locally observed in Fig. 10. However, the large amount of slightly smaller turbines that were built in China leads to a general trend of smaller distances on a global scale. With major offshore wind farm projects being deployed, like the Jiangsu Qidong in 2021, new projects with larger OWT sizes will also reverse this trend in China and eventually globally.

The last attribute, water depth, appears to be stable over the last five years. Until 2021 OWTs are normally bottom-fixed and directly built on structures rammed in the sea ground, known as monopile foundations; tripod or jacket foundations, which are fixated by using caissons or gravity foundations stand directly on the seabed. All of them are used in water depths up to 50 m, as reported in the last row of Fig. 17. Regional differences can be observed between China, the EU and UK. Large parts of the recently built OWTs in China are in nearshore areas with a strong tidal influence and therewith shallow water depth. Even when these areas can also be found in the coastal environments of the EU and UK, they are not used for OWT deployment, primarily due to strict nature reserve regulations of tidal flats.

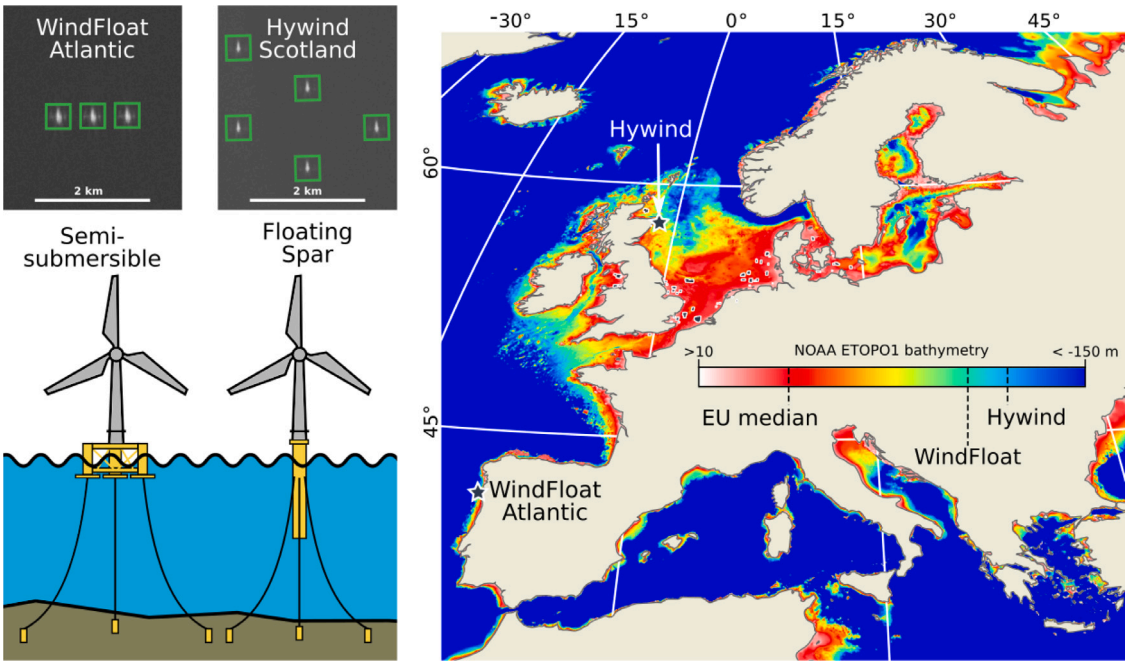

Fig. 18. Two types of floating offshore wind turbines (OWTs) and their application in the pilot projects Hywind in Scotland and WindFloat Atlantic on the Portuguese coast. All turbines are included in the DeepOWT data set, as shown by the green detection boxes. Next to them is the bathymetry of the EU and UK, along with the locations of the two floating offshore wind farm projects. The *EU median* label indicates the median water depth of all OWTs in the EU.

In addition to these general observations regarding water depth, several outliers stand out, both from the temporal and regional perspectives. These outliers do not come from wrong bathymetry estimates of the underlying ETOPO1 data set but are pilot projects of floating offshore wind farms that allow offshore wind turbines to be installed in deeper water depths and with less construction-related impact on the seabed. In 2017 UK's Hywind Scotland floating wind farm was installed in the North Sea Basin, followed by the WindFloat project at the Portuguese Atlantic coast in the EU in 2020, see Fig. 18. These two pilot projects are of major interest since they proved that floating offshore wind farms are technically feasible, and by continuing maturity of this technique and larger project sizes will also become acceptable from an economic perspective (Ramachandran et al., 2021). Floating wind farms will play a major role for the EU since they increase the number of possible offshore wind farm deployment sites (Bento and Fontes, 2019). This is especially important for the Atlantic and Mediterranean coasts (Pustina et al., 2020) with typically steeply sloping water depths compared to the North Sea Basin and Baltic Sea. Fig. 18 provides an overview of the European bathymetry with the water depth given for the two mentioned pilot projects as well as the median water depth of all OWTs in the EU. With the development of new technologies for the offshore wind industry, the EU and UK continue their role as pioneers in this technology.

7. Discussion

In this study, freely available Earth observation and GIS data were used to generate a database, which can provide in-depth information about the development of the offshore wind energy sector on multiple temporal and spatial scales. The comparison with third-party surveys, especially the established reports of the Global Wind Energy Council (Lee and Zhao, 2021, 2020) and Wind Europe (Ramírez et al., 2021) demonstrate that the proposed approach can be used to provide detailed insights into the spatiotemporal evolution of the offshore wind energy sector. The OWT analysis delineates the offshore wind energy sector in a transition phase between decades of reaching maturity and at the beginning of a global expansion of large-scale offshore wind energy production. In addition to that, the still ongoing development of new technologies, like floating wind turbines (Ramachandran et al., 2021), open up future application areas of offshore wind farms (UK Gov., 2021). This will lead to a further increase in offshore wind projects in the long term.

The proposed approaches for calculating the hub height of horizontal axis wind turbines and estimating the installed capacity bring new and important information to already existing and freely available OWT data sets. Thereby the proposed approaches are data set agnostic and only rely on point locations of turbines and the openly accessible Sentinel-1 archive. However, the quality of the OWT data is important for the quality of the derived attributes hub height and installed capacity. The location of the turbine centre has to be as accurate as possible. Shifts in the centre location would directly influence the proposed height calculation and thus the installed capacity. Furthermore, the optimal conditions are met by a data set which provides detailed information about the deployment stage. Without the centre pole and nacelle of an OWT installed, no layover effects appear in the radar imagery, and thus no height calculation can be conducted. Hence, a foundation of an OWT has to be differentiated from a foundation with a turbine on top. The earlier mentioned studies by Wong et al. (2019), Xu et al. (2020) and Zhang et al. (2021) do not differentiate between these deployment stages. By classifying turbine foundations and readily deployed turbines both as operational OWTs, the number of OWTs in these data sets suffers from temporal overestimation, which can be seen in Fig. 16. This overestimation in OWTs would directly influence the estimation of installed capacity based on this number. Thus, the most robust processing and accurate results for height estimation and even more important installed capacity estimation are so far only ensured by combining the proposed approaches with the DeepOWT data set (Hoeser et al., 2022).

The introduced methods for calculating OWT height and installed capacity add important context to the recently proposed DeepOWT data set (Hoeser et al., 2022). The results presented in this study provide insights into technical metrics commonly used to report about developments of the offshore wind energy sector (Lee and Zhao, 2021, 2020; Ramírez et al., 2021; European Commission et al., 2019). In order to provide more insights into the offshore wind energy sector, the data set has to be further discussed and contextualised by adding

expert knowledge from outside the Earth observation and geoinformation domain. With its quarterly frequency, multiple aspects and their spatiotemporal influence on the offshore wind energy sector can be investigated, like the entry into force of legal decisions, new regulations on multi-use policies and nature reserve, price developments in the energy and CO_2 markets, or subsidies for renewable energy (deCastro et al., 2019). Furthermore, the effects of offshore wind infrastructure on marine ecosystems can be investigated more easily when accurate spatiotemporal information is available, especially when their characteristic attributes can be derived from freely available data. All together, the data set and proposed approaches to derive turbine height and installed capacity focus primarily on providing free offshore wind energy infrastructure data for a large scientific community. Freely available data can accelerate the gain of insights, especially in research areas not directly linked to the industry. Nevertheless, their insights are linked indirectly to the offshore wind energy sector. Today, carbon-free and autonomous energy production are already strong arguments for investing in offshore wind energy. However, it is also important to ensure sustainability during the deployment, production and decommissioning phase of offshore wind farms. Without insights gathered by e.g. ecological studies, this crucial component remains underrepresented. With more research in this direction, the involved offshore wind energy industry has the opportunity to adapt practices in order to foster sustainability. Such adaptations that foster sustainable offshore wind energy projects will add additional value to the offshore wind energy industry.

With the upcoming growth of the offshore wind energy sector (Rodrigues et al., 2015), the support of accompanying studies and independent research are of major importance to ensure that all stakeholders are getting involved (Guşatu et al., 2021), and adverse effects are kept to a minimum during a phase of maximising installed capacities in marine and coastal ecosystems. Thus, freely available data is one major building block enabling these essential investigations.

Especially for OWT, the levelised cost of energy is highly sensitive to maintenance measures and OWT downtime (Ren et al., 2021). Well-prepared maintenance measures are necessary to avoid unplanned downtime. Condition monitoring systems are powerful tools to manage maintenance strategies to achieve the highest possible availability at the lowest possible cost for the individual units (Ren et al., 2021; Le and Andrews, 2016). The resulting question is to what extent the data and methods presented can be used to detect and document turbine downtimes and thus support the organisation of maintenance measures.

The 10 m pixel spacing and the six to twelve-day revisit rate of the Sentinel-1 mission show the limits of the applications for which the Sentinel-1 mission can be used. Hence, reliably detecting unplanned OWT downtimes or changes in single components of the OWT is impossible. Only the complete decommissioning of an OWT would be possible since it is a reverse of the construction process, which, as described, can be detected. In order to gain further insights into the operational phase of an OWT, data with a very high spatial and temporal resolution have to be taken into account. Radar missions like TerraSAR-X and ICEYE, both with a spatial resolution of up to 25 cm, and optical missions like WorldView (up to 30 cm) and Skysat (up to 50 cm) provide a spatial resolution which offers the possibility for new applications related to maintenance management. However, only the PlanetScope mission with a daily revisit rate and a spatial resolution of 3 m could provide a sampling frequency which is suitable for such applications. Nevertheless, since PlanetScope operates optical sensor systems, cloud cover will reduce its applicability. Thus, with available methods and sensor systems, today, day-to-day monitoring of single OWTs is not possible from an Earth observation perspective, which demonstrates the current methodological boundaries of what is possible with satellite-based Earth observation data.

As shown in Section 6, shallow water areas near the coast are used for offshore wind energy production in different ways in different regions. Such areas offer favourable conditions, as costs during construction are lower due to reduced logistical effort and less materials for foundations and submarine cables to be used (Kim et al., 2018). However, These areas are often characterised by intensive multiple use by different stakeholders and purposes that mix socio-economic and environmental interests such as fishing, aquaculture, shipping routes, recreational spaces, populated coastal areas, cultural heritage or nature conservation areas (Kim et al., 2018; Russell and Firestone, 2022; Gusatu et al., 2020; Virtanen et al., 2022). Embedding offshore wind energy sites in these already diverse and existing multiple uses of coastal areas poses major planning challenges (Guşatu et al., 2021; Virtanen et al., 2022). Chinese inter tidal offshore wind farm projects in Jiangsu province demonstrate how offshore wind energy infrastructure can be built and operated in multi-use shallow water areas with challenging sediment dynamics (Zhang et al., 2022). With the additional information on OWT level derived in the proposed study, particularly the installed capacity, it is possible to contextualise the spatio-temporal OWT data with socio-economic and ecological data to investigate better the cost–benefit of offshore wind turbines in multi-use shallow water areas.

Recent developments in the offshore wind energy sector have led to the increased demand for floating offshore wind turbines in order to realise offshore wind farms in deep water (Bento and Fontes, 2019). In these environments, floating offshore wind turbines have to withstand different kinds of environmental loads such as regular and irregular waves of changing magnitude (Pustina et al., 2020), aerodynamic loads and strong currents (Shah et al., 2021). Dynamic control measures are necessary to reduce structural loads and maintain optimal performance conditions in these extreme environments (Shah et al., 2021; Gao et al., 2022). Due to the movements of floating offshore platforms in connection with the six to twelve-day recording frequency of the Sentinel-1 mission, the methodology for hub height calculation and capacity estimation must be critically questioned. The following results were obtained for the two, in Fig. 18 introduced, floating offshore wind farm projects, Hywind Scotland and WindFloat Atlantic: The reported (r) and the *estimated (e)* installed capacities are Hywind: 6 MW (r), 6.76 MW ± 0.21 MW (e), WindFloat: 8.4 MW (r), 8.06 MW ±0.89 MW (e). These examples show that the proposed method achieves robust results for floating offshore wind turbines. The explanation lies in the investigation of median composites of all Sentinel-1 acquisitions within a quarter during height calculation. Thus, the approach becomes robust against outliers, which would occur if only a single acquisition had been used.

Future analysis of Earth observation data can build on the proposed workflow and further improve the modelling of installed capacity. The impact of technological improvements on the installed capacity of horizontal axis wind turbines (HAWT) will become greater, making the hub height less significant as the sole indicator. Thus, multiple variables will become necessary to estimate the installed capacity in the future. Primarily attributes provided in this study, such as the date of deployment and minimum distance to the nearest neighbour, can be used potentially. The deployment date is suitable to communicate technological improvements gained over time, and the minimum distance among OWTs is indirectly related to the rotor diameter, a crucial metric for investigating the installed capacity of HAWTs.

An adaptation of the proposed approaches for height calculation and installed capacity estimation must be considered in case new turbine designs are established. Alternative designs such as the vertical axis wind turbine (VAWT) represent entirely different turbine layouts which will also be entirely different in the radar backscatter signal. The procedures presented need to be revised in the situation where a VAWT design has been presented and successfully implemented at a scale comparable to HAWTs. However, the introduced procedures assume the HAWT design, which is currently the only turbine design used for industrial-scale offshore wind farms (Liu et al., 2019; Hand and Cashman, 2020; Mohan Kumar et al., 2019). In general, wind energy

Table A.1
Overview of all calculated metrics to compare the mapping performance of offshore wind turbines of different data sets.

GT group	GT OWTs	Detected OWTs	TP	FP	FN	Pr	Rc	F1
DeepOWT								
North Sea	4016	3997	3996	1	20	1.000	0.995	0.997
East China Sea	2208	2184	2168	16	40	0.993	0.982	0.987
micro avg	6224	6181	6164	17	60	0.997	0.990	0.994
macro avg	6224	6181	6164	17	60	0.997	0.989	0.993
OSM								
North Sea	4016	4038	3581	457	435	0.887	0.892	0.889
East China Sea	2208	384	373	11	1835	0.971	0.169	0.288
micro avg	6224	4422	3954	468	2270	0.894	0.635	0.743
macro avg	6224	4422	3954	468	2270	0.917	0.565	0.640
GOWTv1.3								
North Sea	3571	3496	3332	164	239	0.953	0.933	0.943
East China Sea	1208	1233	1149	84	59	0.932	0.951	0.941
micro avg	4779	4729	4481	248	298	0.948	0.938	0.943
macro avg	4779	4729	4481	248	298	0.944	0.941	0.942
GOWTv2021								
North Sea	4016	4483	3965	518	51	0.884	0.987	0.933
East China Sea	2208	3649	2080	1569	128	0.570	0.942	0.710
micro avg	6224	8132	6045	2087	179	0.743	0.971	0.842
macro avg	6224	8132	6045	2087	179	0.733	0.967	0.828

production has a broad field of potential generator layouts. We refer to Roga et al. (2022) for a recent review of different types of generator layouts. Due to the potential introduction of new generator designs into the offshore wind sector and changes in the established HAWT design, it is necessary to refine the approach of estimating the installed capacity continuously. This is an ongoing task for future research in order to consolidate the global monitoring of the offshore wind energy sector with Earth observation data.

8. Conclusion

This study proposes an approach to calculate the hub height of offshore wind turbines (OWTs) and to estimate their corresponding installed capacity on a global scale. The entire process is based on freely available Earth observation and GIS data. The recently proposed global data set of OWTs, the DeepOWT data set (Hoeser et al., 2022), and the Sentinel-1 archive. Further site specifications of OWTs were obtained and used to provide a spatiotemporal analysis of the recent evolution of the offshore wind energy sector.

Between July 2016 and June 2021 additional 5268 OWTs with a derived cumulative capacity of 27.2 GW were deployed worldwide. Together, the cumulative installed capacity in June 2021 was 40.6 GW provided by 8885 OWTs. Thus within the investigated five years, the installed capacity was increased by 200%. The three major contributors are the European Union (EU) (3096 OWTs and 15.2 GW), China (3267 OWTs and 14.1 GW), and the United Kingdom (UK) (2378 OWTs and 10.7 GW). China had the highest growth rate with 13 GW and 2960 OWTs. In the same period, the offshore wind sector in the EU and UK grew by 8 GW and 1313 OWTs, and 5.8 GW and 916 OWTs, respectively. Most OWTs were deployed and are still under construction in the North Sea Basin and the East and the South China Sea. With new technologies like floating wind farms, water depths deeper as 50 m will become accessible in future. The deepest depth of 110 m is of the European pilot project Hywind Scotland.

A progressively larger distance between recently deployed OWTs and the shoreline indicates that at established regions of wind energy production, potential offshore areas close to the coast have already been exploited. This aspect and the high number of recently constructed artificial objects in marine ecosystems make it obvious that integrated planning that includes all stakeholders involved in coastal and marine space is necessary. Future research that further investigates the proposed methods and data is necessary to add expert knowledge from other domains to ensure that carbon-neutral energy production with offshore wind turbines is as sustainable as possible.

CRediT authorship contribution statement

Thorsten Hoeser: Designed the study, Collected the ground truth data, Developed and implemented the code for data processing, Visualisation, Evaluation, Writing – original draft, Writing – review & editing. **Claudia Kuenzer:** Supervised the study, Gave suggestions for figures, Repeatedly commented, Discussed the manuscript, Writing – review & editing.

Declaration of competing interest

The authors declare that they have no known competing financial interests or personal relationships that could have appeared to influence the work reported in this paper.

Data availability

A link to the data repository is provided in Appendix B.

Acknowledgements

The authors would like to thank ESA's Copernicus programme for providing free access to the Sentinel-1 data and the Google Earth Engine platform for preprocessing and making the data accessible. Furthermore, we would like to thank the OpenStreetMap project for providing offshore wind turbine locations. We would like to thank Achim Roth for a fruitful conversation about the geometric interpretation of the radar signal. Finally we would like to thank the two anonymous reviewers for their valuable comments.

Funding

This research did not receive any specific grant from funding agencies in the public, commercial, or not-for-profit sectors.

Appendix A. F1 score calculation for OWT mapping of different data sets

Fig. 3(b) compares freely accessible data sets which contain offshore wind turbine (OWT) locations. The comparison provides insights into the mapping performance of the different data sets. To compare these data sets quantitatively, they were assessed on manually labelled data of the two most important offshore wind energy production sites, the North Sea Basin and the East China Sea. The employed ground truth data sets originate from Hoeser et al. (2022) and can be downloaded from https://zenodo.org/record/5933967.

The data sets reviewed are the DeepOWT data set , OWT locations from the Open Street Map (OSM) database and the global offshore wind turbine data set (GOWT) presented by Zhang et al. (2021), in its original version (v1.3) and the current version after the latest update (v2021). All data sets, except GOWT v1.3, were compared with the ground truth datasets describing the status at the end of the second quarter of 2021. For GOWT v1.3, ground truth datasets were used, which show the status at the end of the fourth quarter of 2019. All data sets to be checked have been prepared to show OWTs detected until the respective ground truth date. Furthermore, a spatial subset of all data sets was made based on the boundaries of the ground truth test sites, the North Sea Basin and the East China Sea. These Polygons are also included in the ground truth repository referenced above.

Following this, the F1 scores were calculated for each data set, grouped by the two ground truth test sites (North Sea Basin and East China Sea). For a subsequent combination of both test sites, the macro averaging method was used to prevent an overrepresentation of the numerically more represented OWTs from the North Sea Basin test site, where conditions are easier than in the East China Sea due to the stage and dynamics of the offshore wind energy sector development, coastal

Fig. A.19. Definition of True Positive (TP), False Positive (FP) and False Negative (FN) for mapped offshore wind turbine (OWT) locations.

morphology and location of offshore wind farms. However, to provide a complete picture, also the micro average F1 scores have been calculated and are provided with all other metrics in Table A.1.

Fig. A.19 gives an overview of the Definitions of True Positives (TP), False Positives (FP) and False Negatives (FN). If an OWT location is within a radius of 100 m of a ground truth OWT location, this mapped location is considered a TP. If a mapped OWT location lies outside this radius, the location is defined as FP. If there is a ground truth location without a mapped OWT location within a radius of 100 m, it is defined as FN.

The following equations were used to calculate the metrics (Precision (Pr), Recall (Rc)):

$$\mathrm{Pr} = \frac{\mathrm{TP}}{\mathrm{TP} + \mathrm{FP}} \tag{A.1}$$

$$\mathrm{Rc} = \frac{\mathrm{TP}}{\mathrm{TP} + \mathrm{FN}} \tag{A.2}$$

$$\mathrm{F1} = 2 \times \frac{\mathrm{Pr} \times \mathrm{Rc}}{\mathrm{Pr} + \mathrm{Rc}} \tag{A.3}$$

$$\mathrm{Pr}_{\mathrm{macro-avg}} = \frac{1}{n} \sum_{i=1}^{n} \mathrm{Pr}_i \tag{A.4}$$

$$\mathrm{Rc}_{\mathrm{macro-avg}} = \frac{1}{n} \sum_{i=1}^{n} \mathrm{Rc}_i \tag{A.5}$$

$$\mathrm{F1}_{\mathrm{macro-avg}} = \frac{1}{n} \sum_{i=1}^{n} \mathrm{F1}_i \tag{A.6}$$

Table A.1 holds all calculated metrics grouped by data set and test site.

Appendix B. Supplementary data

The Zenodo repository https://doi.org/10.5281/zenodo.6903489 contains:

- `supplementary_data_B_OWT_height_capacity.csv` - Train/test offshore wind turbine height and installed capacity values
- `supplementary_data_B_DeepOWT_1_21_2_plus.geojson` - Extended version of the DeepOWT data set (https://zenodo.org/record/5933967) by all of the derived attributes in this study e.g. OWT hub height and installed capacity.

References

Amante, C., Eakins, B.W., 2009. Etopo1 1 arc-minute global relief model: Procedures, data sources and analysis. In: NOAA Technical Memorandum NESDIS NGDC-24. http://dx.doi.org/10.7289/V5C8276M, URL: https://www.ngdc.noaa.gov/mgg/global/global.html.

Bento, N., Fontes, M., 2019. Emergence of floating offshore wind energy: Technology and industry. Renew. Sustain. Energy Rev. 99, 66–82.

COP26, 2021a. Global coal to clean power transition statement. URL: https://ukcop26.org/global-coal-to-clean-power-transition-statement/.

COP26, 2021b. Zero emission vehicles transition council: 2022 action plan. URL: https://ukcop26.org/zero-emission-vehicles-transition-council-2022-action-plan/.

deCastro, M., Salvador, S., Gómez-Gesteira, M., Costoya, X., Carvalho, D., Sanz-Larruga, F., Gimeno, L., 2019. Europe, China and the united states: Three different approaches to the development of offshore wind energy. Renew. Sustain. Energy Rev. 109, 55–70.

EC, E.C., 2020. An EU strategy to harness the potential of offshore renewable energy for a climate neutral future. URL: https://ec.europa.eu/energy/sites/ener/files/offshore_renewable_energy_strategy.pdf.

European Commission, Joint Research Centre, Vazquez Hernandez, C., Telsnig, T., 2019. Wind Energy : Technology Market Report. Publications Office, http://dx.doi.org/10.2760/260914.

Flanders Marine Institute, 2020. Union of the ESRI country shapefile and the exclusive economic zones (version 3). http://dx.doi.org/10.14284/403, URL: https://www.marineregions.org/.

Gao, Z.T., Feng, X.Y., Zhang, Z.T., Liu, Z.L., Gao, X.X., Zhang, L.J., Li, S., Li, Y., 2022. A brief discussion on offshore wind turbine hydrodynamics problem. J. Hydrodyn. 34, 15–30. http://dx.doi.org/10.1007/s42241-022-0002-y.

Gorelick, N., Hancher, M., Dixon, M., Ilyushchenko, S., Thau, D., Moore, R., 2017. Google earth engine: Planetary-scale geospatial analysis for everyone. Remote Sens. Environ. 202, 18–27. http://dx.doi.org/10.1016/j.rse.2017.06.031, Big remotely sensed data: Tools, applications and experiences.

Guşatu, L., Menegon, S., Depellegrin, D., Zuidema, C., Faaij, A., Yamu, C., 2021. Spatial and temporal analysis of cumulative environmental effects of offshore wind farms in the north sea basin. Sci. Rep. 11, http://dx.doi.org/10.1038/s41598-021-89537-1.

Gusatu, L.F., Yamu, C., Zuidema, C., Faaij, A., 2020. A spatial analysis of the potentials for offshore wind farm locations in the north sea region: Challenges and opportunities. ISPRS Int. J. Geo-Inf. 9 (96), http://dx.doi.org/10.3390/ijgi9020096.

Hand, B., Cashman, A., 2020. A review on the historical development of the lift-type vertical axis wind turbine: From onshore to offshore floating application. Sustain. Energy Technol. Assess. 38, 100646. http://dx.doi.org/10.1016/j.seta.2020.100646.

Hoeser, T., Bachofer, F., Kuenzer, C., 2020. Object detection and image segmentation with deep learning on earth observation data: A review—part II: Applications. Remote Sens. 12, http://dx.doi.org/10.3390/rs12183053.

Hoeser, T., Feuerstein, S., Kuenzer, C., 2022. DeepOWT: A global offshore wind turbine data set derived with deep learning from sentinel-1 data. Earth Syst. Sci. Data Discuss. 2022, 1–26. http://dx.doi.org/10.5194/essd-2022-115.

Hoeser, T., Kuenzer, C., 2020. Object detection and image segmentation with deep learning on earth observation data: A review-part i: Evolution and recent trends. Remote Sens. 12, http://dx.doi.org/10.3390/rs12101667.

Hoeser, T., Kuenzer, C., 2022. SyntEO: Synthetic dataset generation for earth observation and deep learning – demonstrated for offshore wind farm detection. ISPRS J. Photogramm. Remote Sens. 189, 163–184. http://dx.doi.org/10.1016/j.isprsjprs.2022.04.029.

Kim, C.K., Jang, S., Kim, T.Y., 2018. Site selection for offshore wind farms in the southwest coast of South Korea. Renew. Energy 120, 151–162. http://dx.doi.org/10.1016/j.renene.2017.12.081.

Le, B., Andrews, J., 2016. Modelling wind turbine degradation and maintenance. Wind Energy 19, 571–591. http://dx.doi.org/10.1002/we.1851.

Lee, J., Zhao, F., 2020. GWEC - Global Wind Report 2019. Global Wind Energy Council, URL: https://gwec.net/global-wind-report-2019/.

Lee, J., Zhao, F., 2021. GWEC - Global Wind Report 2021. Global Wind Energy Council, URL: https://gwec.net/global-wind-report-2021/.

Liu, J., Lin, H., Zhang, J., 2019. Review on the technical perspectives and commercial viability of vertical axis wind turbines. Ocean Eng. 182, 608–626. http://dx.doi.org/10.1016/j.oceaneng.2019.04.086.

Ma, L., Liu, Y., Zhang, X., Ye, Y., Yin, G., Johnson, B.A., 2019. Deep learning in remote sensing applications: A meta-analysis and review. ISPRS J. Photogramm. Remote Sens. 152, 166–177. http://dx.doi.org/10.1016/j.isprsjprs.2019.04.015.

Meric, S., Fayard, F., Pottier, E., 2009. Radargrammetric sar image processing. In: Ho, P.G.P. (Ed.), Geoscience and Remote Sensing. IntechOpen, Rijeka, http://dx.doi.org/10.5772/8300, (Chapter 20).

Mohan Kumar, P., Sivalingam, K., Lim, T.C., Ramakrishna, S., Wei, H., 2019. Review on the evolution of darrieus vertical axis wind turbine: Large wind turbines. Clean Technol. 1, 205–223. http://dx.doi.org/10.3390/cleantechnol1010014.

Natural Earth, 2022. 1:10 m physical vectors. URL: https://www.naturalearthdata.com/downloads/10m-physical-vectors/.

Pustina, L., Lugni, C., Bernardini, G., Serafini, J., Gennaretti, M., 2020. Control of power generated by a floating offshore wind turbine perturbed by sea waves. Renew. Sustain. Energy Rev. 132, 109984. http://dx.doi.org/10.1016/j.rser.2020.109984.

Ramachandran, R. Chitteth, Desmond, C., Judge, F., Serraris, J.J., Murphy, J., 2021. Floating offshore wind turbines: Installation, operation, maintenance and decommissioning challenges and opportunities [preprint]. Wind Energy Sci. Discuss. 2021, 1–32.

Ramírez, L., Fraile, D., Brindley, G., O'Sullivan, R., Miró, L., de Velde, L.V., 2021. Offshore Wind in Europe - Key Trends and Statistics 2020. Wind Europe, URL: https://windeurope.org/intelligence-platform/product/offshore-wind-in-europe-key-trends-and-statistics-2020/.

Ren, Z., Verma, A.S., Li, Y., Teuwen, J.J., Jiang, Z., 2021. Offshore wind turbine operations and maintenance: A state-of-the-art review. Renew. Sustain. Energy Rev. 144, 110886. http://dx.doi.org/10.1016/j.rser.2021.110886.

Rodrigues, S., Restrepo, C., Kontos, E., Teixeira Pinto, R., Bauer, P., 2015. Trends of offshore wind projects. Renew. Sustain. Energy Rev. 49, 1114–1135. http://dx.doi.org/10.1016/j.rser.2015.04.092.

Roga, S., Bardhan, S., Kumar, Y., Dubey, S.K., 2022. Recent technology and challenges of wind energy generation: A review. Sustain. Energy Technol. Assess. 52, 102239. http://dx.doi.org/10.1016/j.seta.2022.102239.

Russell, A., Firestone, J., 2022. More than a feeling: Analyzing community cognitive and affective perceptions of the block island offshore wind project. Renew. Energy 193, 214–224. http://dx.doi.org/10.1016/j.renene.2022.05.032.

Shah, K.A., Meng, F., Li, Y., Nagamune, R., Zhou, Y., Ren, Z., Jiang, Z., 2021. A synthesis of feasible control methods for floating offshore wind turbine system dynamics. Renew. Sustain. Energy Rev. 151, 111525. http://dx.doi.org/10.1016/j.rser.2021.111525.

Smirnov, N.V., 1939. Estimate of deviation between empirical distribution functions in two independent samples. Bull. Mosc. Univ. 2, 3–16.

Statista, 2021a. Global offshore wind energy capacity from 2009 to 2020. URL: https://www.statista.com/statistics/476327/global-capacity-of-offshore-wind-energy/.

Statista, 2021b. Wichtigste Länder weltweit nach installierter offshore-windenergieleistung im Jahr 2020. URL: https://de.statista.com/statistik/daten/studie/158501/umfrage/kapazitaeten-der-offshore-windkraft-nach-laendern-im-jahr-2009/.

Torres, R., Snoeij, P., Geudtner, D., Bibby, D., Davidson, M., Attema, E., Potin, P., Rommen, B., Floury, N., Brown, M., Traver, I.N., Deghaye, P., Duesmann, B., Rosich, B., Miranda, N., Bruno, C., L'Abbate, M., Croci, R., Pietropaolo, A., Huchler, M., Rostan, F., 2012. Gmes sentinel-1 mission. Remote Sens. Environ. 120, 9–24. http://dx.doi.org/10.1016/j.rse.2011.05.028.

UK Gov., 2021. Net Zero Strategy: Build Back Greener. HM Government, London, URL: https://assets.publishing.service.gov.uk/government/uploads/system/uploads/attachment_data/file/1033990/net-zero-strategy-beis.pdf.

Virtanen, E., Lappalainen, J., Nurmi, M., Viitasalo, M., Tikanmäki, J., Atlaskin, E., Kallasvuo, M., Tikkanen, H., Moilanen, A., 2022. Balancing profitability of energy production, societal impacts and biodiversity in offshore wind farm design. Renew. Sustain. Energy Rev. 158, 112087. http://dx.doi.org/10.1016/j.rser.2022.112087.

Wikipedia, 2022. Liste der offshore-windparks. URL: https://de.wikipedia.org/wiki/Liste_der_Offshore-Windparks.

Wong, B.A., Thomas, C., Halpin, P., 2019. Automating offshore infrastructure extractions using synthetic aperture radar and Google earth engine. Remote Sens. Environ. 233, 111412. http://dx.doi.org/10.1016/j.rse.2019.111412.

Xu, W., Liu, Y., Wu, W., Dong, Y., Lu, W., Liu, Y., Zhao, B., Li, H., Yang, R., 2020. Proliferation of offshore wind farms in the north sea and surrounding waters revealed by satellite image time series. Renew. Sustain. Energy Rev. 133, 110167. http://dx.doi.org/10.1016/j.rser.2020.110167.

Zhang, T., Tian, B., Sengupta, D., Zhang, L., Si, Y., 2021. Global offshore wind turbine dataset. Sci. Data 8, http://dx.doi.org/10.1038/s41597-021-00982-z.

Zhang, H., Zhang, D., Zhou, Y., Cutler, M.E.J., Cui, D., Zhang, Z., 2022. Quantitative analysis of the interaction between wind turbines and topography change in intertidal wind farms by remote sensing. J. Mar. Sci. Eng. 10, http://dx.doi.org/10.3390/jmse10040504.

Zhu, X.X., Tuia, D., Mou, L., Xia, G., Zhang, L., Xu, F., Fraundorfer, F., 2017. Deep learning in remote sensing: A comprehensive review and list of resources. IEEE Geosci. Remote Sens. Mag. 5, 8–36.